The Circadian Clock is Disrupted in Pancreatic Cancer

Authors: Patrick B. Schwartz, MD[1], Manabu Nukaya, PhD[1], Mark Berres, PhD[2], Clifford D. Rubinstein, PhD[2], Gang Wu, PhD[3], John B. Hogenesch, PhD[3], Christopher A. Bradfield, PhD[4], and Sean M. Ronnekleiv-Kelly, MD[1,5]

Affiliations:

[1]Department of Surgery, Division of Surgical Oncology, University of Wisconsin School of Medicine and Public Health, Madison, WI

[2]Biotechnology Center, University of Wisconsin, Madison, WI

[3]Division of Human Genetics and Immunobiology, Center for Circadian Medicine, Department of Pediatrics, Cincinnati Children's Hospital Medical Center, Cincinnati, Ohio

[4]McArdle Laboratory for Cancer Research, Department of Oncology, University of Wisconsin School of Medicine and Public Health, Madison, WI

[5]University of Wisconsin Carbone Cancer Center, University of Wisconsin School of Medicine and Public Health, Madison, WI

Corresponding Author: Sean M Ronnekleiv-Kelly, MD (ronnekleiv-kelly@surgery.wisc.edu)

Address: 600 Highland Ave. Bx 7375, K3/705 CSC, Madison, WI, 53792

Phone: (608) 262-2025 **Fax:** (608) 252-0913

Running Title: Pancreatic Cancer Clock

Funding: The research reported in this publication was supported by the Department of Defense Peer Reviewed Cancer Research Program Idea Award Number CA190176 (Grants.gov ID GRANT12935023) (SRK), by the National Institutes of Health (NIH) National Institute of Environmental Health Sciences (NIEHS) Award Number R35ES028377 (CAB), by the NIH NIEHS Award Number T32 ES007015

(PBS) and the University of Wisconsin Carbone Cancer Center (SRK). The content is solely the responsibility of the authors and does not necessarily represent the official views of the Department of Defense or the National Institutes of Health.

Disclosure: The authors declare no conflict of interest or competing interests

Abstract

Disruption of the circadian clock is inextricably linked to cancer development and progression. Establishing this connection has proven beneficial for understanding cancer pathogenesis, determining prognosis, and uncovering novel therapeutic targets. However, barriers to characterizing the circadian clock in human pancreas and human pancreatic cancer – one of the deadliest malignancies – have hindered an appreciation of its role in this cancer. Here, we employed normalized coefficient of variation (nCV) and clock correlation analysis in human population-level data to determine the functioning of the circadian clock in pancreas cancer and adjacent normal tissue. We found a substantially attenuated clock in the pancreatic cancer tissue. Then we exploited our existing mouse pancreatic transcriptome data to perform an analysis of the human normal and pancreas cancer samples using a machine learning method, cyclic ordering by periodic structure (CYCLOPS). Through CYCLOPS ordering, we confirmed the nCV and clock correlation findings of an intact circadian clock in normal pancreas with robust cycling of several core clock genes. However, in pancreas cancer, there was a loss of rhythmicity of many core clock genes with an inability to effectively order the cancer samples, providing substantive evidence of a dysregulated clock. The implications of clock disruption were further assessed with a *Bmal1* knockout pancreas cancer model, which revealed that an arrhythmic clock caused accelerated cancer growth and earlier metastatic spread, accompanied by chemoresistance and enrichment of key cancer-related pathways. These findings provide strong evidence for clock disruption in human pancreas cancer and demonstrate a link between circadian disruption and pancreas cancer progression.

Introduction

The circadian clock is a conserved molecular feedback loop that regulates many signaling pathways to control metabolism, immunity, apoptosis, and other critical cellular functions in the body.[1] At its core, the positive arm of the clock (i.e. CLOCK and BMAL1 [also known as ARNTL or MOP3]) drives transcription of the negative arm, including PER1-3 and CRY1-2.[2,3] The negative arm represses the transcriptional activation of CLOCK and BMAL1, and a second interlocked loop involves the nuclear receptors RORα/β/λ and NR1D1-2 (also known as REV-ERBα/β), which activate and suppress BMAL1 expression, respectively. These, along with other core clock components, form a tightly regulated series of transcriptional-translational feedback loops that ensure rhythmic expression over 24 hours and function to maintain cellular and organ homeostasis.[2–4]

Environmental cues influence the synchronization of circadian rhythms in various organ systems, and misalignment of external cues with the internal clock (e.g. shift work) can cause clock dysfunction with consequent metabolic derangements and pathologic states.[4–6] For instance, circadian dysregulation has been strongly linked to obesity and diabetes, both risk factors for cancer.[7–11] Concordantly, landmark studies have shown that disruption of the endogenous clock through mutations in or suppression of the core clock genes is intricately linked to tumor growth in several cancers.[12–14] For example, knockout of *Bmal1* in *Kras*- and *p53*-mutant lung cancer causes marked tumor progression *in vivo*,[13] while MYC-induced repression of *BMAL1* in human neuroblastoma drives decreased overall survival in a BMAL1-dependent manner.[15] Importantly, targeting dysfunctional clock components in certain cancers has proven an effective treatment strategy.[15,16] Thus, identifying an aberrantly functioning circadian clock in cancer can lead to key advancements such as understanding pathogenesis, prognosis, and uncovering novel therapeutic targets.

Although indeterminate, there is some evidence that the clock may be dysregulated in pancreatic ductal adenocarcinoma (PDAC), leading to a worse prognosis;[17,18] this is alarming for a deadly malignancy where only 11% of patients survive beyond 5 years.[19] To advance our understanding of how clock

disruption impacts PDAC pathogenesis, and ultimately foster the identification of therapeutic targets, an essential first step is to establish that clock dysfunction exists in human PDAC. Unfortunately, to date, the cumulative data does not definitively support this assertion and is inconclusive. Prior studies have relied on contrasting expression differences between the core clock genes in tumor compared to normal pancreas as a basis for clock disruption.[17,18,20,21] But differential expression alone is limited, and does not provide insight into critical components of clock health such as relative amplitude, rhythmicity, or correlation of expression amongst core clock genes.[22] Moreover, in the pancreas, phase advancement as a result of chronic jetlag causes differential expression of core clock genes while maintaining a robust and healthy clock (i.e. strong relative amplitude, rhythmicity, and clock correlation).[23] Thus, much more substantive data is required to affirm clock disruption in PDAC.

In pre-clinical studies (e.g. mouse or cell-line models), the determinants of clock health can be identified by obtaining longitudinal data under controlled conditions.[23,24] However, in human studies – particularly human pancreas – the requisite periodic data by multiple sampling is not feasible (or ethical). Therefore, alternative means of determining rhythmically expressed genes in humans are necessary. Following the emergence of several bioinformatics tools, the principal aspects of clock health including relative amplitude, core clock gene correlation, and statistical determination of rhythmicity can be resolved when using the appropriate reference data.[22,25–28] We recently generated a robust pancreas dataset demonstrating diurnally expressed genes over 48 hours.[23] With this foundation, we were able to apply normalized coefficient of variation (nCV), clock correlation analysis, and cyclic ordering by periodic structure (CYCLOPS) to test the hypothesis that the circadian clock is disrupted in human PDAC.[22,25,28] While on the surface this may be construed as a simplistic hypothesis, several limitations have hindered the ability to evaluate the circadian clock in human pancreas, including the lack of human periodic data and an absence of a reference transcriptional dataset.

Here, we employed nCV, clock correlation analysis, and CYCLOPS on publicly available human population-level expression data from The Cancer Genome Atlas (TCGA) and Clinical Proteomic Tumor

Analysis Consortium 3 (CPTAC-3) datasets to determine the health of the circadian clock in PDAC and adjacent normal tissue.[29,30] For the first time, we identified an intact circadian clock in human normal pancreas with robust cycling of several core clock genes. We also found a markedly weakened clock in the cancer tissue, providing substantive evidence of a dysregulated clock in PDAC. These findings represent significant advancements in evaluating clock function in PDAC, and the potential clinical implications of clock disruption were further assessed with a pre-clinical PDAC model. We used CRISPR/Cas9 technology to selectively target *Bmal1* and examined the effects of clock dysfunction *in vitro* and *in vivo*. This revealed that loss of clock function caused accelerated cancer growth, earlier metastatic spread, enrichment of key cancer-related pathways, and resistance to commonly used cytotoxic chemotherapies for PDAC. These findings provide strong evidence for circadian clock disruption in human PDAC and demonstrate a link between circadian disruption and pancreas cancer progression.

Materials and Methods

Mouse Care

All animal studies were conducted according to an approved protocol (M005959) by the University of Wisconsin School of Medicine and Public Health (UW SMPH) Institutional Animal Care and Use Committee (IACUC). Male and female C57BL/6J mice were housed in an Assessment and Accreditation of Laboratory Animal Care (AALAC) accredited selective pathogen-free facility (UW Medical Sciences Center) on corncob bedding with chow diet (Mouse diet 9F 5020; PMI Nutrition International) and water ad libitum. All *in vivo* experiments were performed with age-, cage-, and sex-matched mice under identical lighting conditions.

Clock Correlation, nCV, and CYCLOPS Pipeline

We assessed the overall clock gene correlation and robustness of the clock with the clock correlation matrix and normalized coefficient of variation (nCV) – nCV is known to be correlated with the relative amplitude (rAMP) of oscillating clock genes, indicating the clock robustness.[22,25] The nCV was calculated

for the overall condition with the nCVnet and nCVgene functions.[25] Clock correlation matrices were created using an available shiny app (https://github.com/gangwug/CCMapp) which compares the correlation of clock components (17 individual clock genes) to a baseline correlation from the circadian atlas using the Mantel test.[22,26,27,31,32]

Cyclic ordering by periodic structure (CYCLOPS)[28] was validated for use in the pancreas utilizing our existing murine normal circadian and chronic jetlag pancreas RNA sequencing (RNA-seq) data (Gene Expression Omnibus (GEO) Accession number: GSE165198).[23] Specifically, the seed genes for use in CYCLOPS were selected by cross-referencing genes found to be rhythmically expressed in our dataset with those genes either rhythmically expressed in the liver (similarly metabolic organ) or those used by Wu *et al.* when validating CYCLOPS in the skin (**Supplemental Data File 1**).[23,26,31,32] The updated CYCLOPS pipeline by Wu *et al*. (https://github.com/gangwug/Oslops) was then used to reorder our murine pancreas datasets with known sample collection times.[26] Eigengenes were selected with the Oscope package to sharpen CYCLOPS.[33] Clusters with a $p < 0.05$ and $Met^{smooth} < 1$ were considered to be significantly reordered.[28] Rhythmicity of the reordered genes was determined on cosinor analysis with a $p < 0.01$, rAMP > 0.1, goodness of fit (rsq) > 0.1, and fitmean > 16.[26] Significantly rhythmic gene phase was then compared to the rhythmic gene phase detected from the known sample time collection using the meta3d function of Metacyle.[34] Clock genes were highlighted to demonstrate a correlation between the predicted and actual phase.

The clock was evaluated in human normal and human PDAC RNA-seq datasets from TCGA and CPTAC-3.[29,30] After batch correction with ComBat and filtering, 50 matched normal and 318 PDAC samples were obtained for analysis.[35] The pipeline described above was then used to obtain the clock correlation matrix, nCV, and CYCLOPS reordering. Cosinor analysis was performed to test for rhythmicity. Given the additional biologic heterogeneity of the human data, a $p < 0.05$, rAMP > 0.1, goodness of fit (rsq) > 0.1, and fitmean > 16 were used as a rhythmicity cutoff. Rhythmic genes from normal samples were assessed with phase set enrichment analysis (PSEA).[36] Rhythmic gene sets ordered

by significance were inputted with their calculated phase of expression. Default settings were used for PSEA, including domain 0-24, min item 10, max sims/test 10,000. The gene set enrichment analysis (GSEA) gene ontology (GO) (c5.go.bp.v7.5.1.symbols) set was leveraged as the pathway input. The top 15 significant pathways ($q < 0.05$) were selected for representation.

KPC Cell Line Creation and Maintenance

Pancreas cancer cells that harbor *Kras*^{G12D} and *Trp53*^{R172H} mutations (KPC cells) were acquired from Ximbio (Catalog: 153474; Westfield Stratford City, UK). Cells were cultured in DMEM supplemented with 10% Fetal Bovine Serum (Cytiva, Marlborough, MA), 1% L-glutamate-Penicillin-Streptomycin (Gibco, ThermoFisher Scientific, Waltham, MA), and 1% non-essential amino acids (Gibco) at 37°C at 5.0% CO_2 to their appropriate confluence for use. CRISPR/Cas9 technology was used to introduce *Bmal1* mutations into the well-established KPC cells, generating the *Bmal1* functional knockout line (KPC-BKO).[37] Synthetic tracrRNA and target-specific crRNAs (crRNA:tracrRNA (ctRNAs)) were annealed as per manufacturer instructions (Integrated DNA Technologies (IDT), Coralville, IA). Ribonucleoproteins were formed with Cas9 protein (V3, Catalog: 1081059, IDT) and ctRNAs individually (ctRNA 1:AATATGCAGAACACCAAGGA, ctRNA 2: TTAGAATATGCAGAACACCA) (IDT). Nucleofection was used to introduce RNPs (1.95 µM Cas9, 2 µM ctRNA, 2 µM electroporation enhancer (IDT)) into 2 x 10^5 KPC cells on a Nucleofector 4D (Lonza Biosciences, Walkersville, MD) with an SF kit (Catalog: V4CX-2032, Lonza Biosciences) as per manufacturer instructions using pulse code CM-120. After 48 hours of recovery in DMEM growth media (described above) at 37°C at 5.0% CO_2, single cells were deposited in 96 well plates using a BD FACSAria III (BD Biosciences, Franklin Lakes, NJ). Outgrowing clones were condensed to a 96 well plate in duplicate to propagate clones and generate a genomic DNA source. Genomic DNA was harvested from KPC cells, nucleofected with ctRNA-1 RNPs and ctRNA-2 RNPs, and the targeted region of *Bmal1* was PCR amplified using primers: Forward: acactctttccctacacgacgctcttccgatct NNNNNN CCAAGAATCCTTGTGTGTCTG and Reverse: gtgactggagttcagacgtgtgctcttccgatct AGAGGACTCCACAGACATGAAC (IDT). PCR products were

dual-indexed with indexing PCR, pooled, sequenced on an Illumina MiSeq instrument (San Diego, CA), and analyzed with CRISPResso2.[38]

Creation of Per2-dLuciferase reporter KPC cell line

KPC cells were stably transfected with a mammalian gene expression vector harboring a destabilized luciferase reporter driven by the *Per2* promoter fused to intron 2 of *Per2* and a puromycin resistance cassette (VectorBuilder, Santa Clara, CA).[39] The vector was transfected with lipofectamine 2000 (ThermoFisher Scientific) and incubated for 2 days, and then exposed to media containing 2.5 μg/mL puromycin for 3 days, and surviving clones were selected. Luciferase activity was measured in the selected clones with the luciferase assay system (Promega, Madison, WI) on a BMG CLARIOstar (BMG Labtech, Ortenberg, Germany) plate reader. The two selected clones were then subcloned using a BD FACSAria III after staining with DAPI. Luciferase activity was again measured in the subclones to validate expression before use in downstream experiments.

Clock Function Testing

To evaluate for clock function, KPC and KPC-BKO cells were synchronized with 200 nM dexamethasone for 2 hours in FBS-free DMEM media, followed by RNA isolation 24 hours after the synchronization using the RNeasy protocol (Qiagen, Hilden, Germany) according to the manufacturer's recommendations.[40] Samples (n = 3 biologic replicates) were collected at 4-hour intervals for 24 hours. Quantitative real-time polymerase chain reaction (RT-qPCR) was performed (in technical triplicate) for the downstream core clock gene (CCG) *Per1* (ID: Mm00501813_m1, Life Technologies, Carlsbad, CA) and the housekeeper gene *Hprt* (ID: Mm03024075_m1) using GoTaq® Probe qPCR and RT-qPCR System (Promega, Madison, WI) and Quantstudio 7 flex RT-PCR system (ThermoFisher Scientific). Expression was measured and the ΔCT was calculated. The mean ΔCT values were then tested for rhythmicity using the meta2d function of Metacycle.[34] For Metacycle settings, the min period and max period were set to 24, and “JTK”, “LS”, and “ARS” were selected for cycMethod. An integrated FDR

corrected *q* value < 0.05 and rAMP > 0.1 were taken as rhythmic as previously described.[26] To separately evaluate clock function in KPC cells, luciferase activity driven by the *Per2* promoter was measured. Cells from two independent clones were synchronized with 200 nM dexamethasone for 2 hours in FBS-free DMEM media, and 24 hours later luciferase activity was measured at 4-hour intervals. To measure activity, 1x cell culture lysis reagent (Promega) was added and cells were incubated for 5 minutes. Firefly luciferase assay reagent (Promega) was added and luminescence was measured on a BMG CLARIOstar plate reader and tested for rhythmicity using Metacycle.

Western Blotting

Western blotting was performed to determine BMAL1 expression in two independent KPC cell lines. After synchronization, protein samples were isolated at 6-hour intervals for 24 hours using CelLytic M lysis reagent (MilliporeSigma, Burlington, MA) and Halt Protease and Phosphatase Inhibitor Cocktail (ThermoFisher Scientific). A total of 30 μg of each sample was loaded onto a Mini-PROTEAN TGX 7.5% precast mini-gel (Bio-RAD Laboratories, Hercules, CA). The gel was then transferred using the semi-dry transfer technique to an Immobilon-P PVDF membrane (MilliporeSigma). The membrane was then blocked with 5% skim milk and incubated with 1 μg/μL rabbit BMAL1 antibody (Catalog: NB100-2288, RRID: AB_10000794, Novus Biologicals, Littleton, CO) and 1:2000 rabbit β-ACTIN antibody (Catalog: 4967, RRID: AB_330288, Cell Signaling Technologies, Danvers, MA). Finally, the membranes were incubated with alkaline phosphatase-conjugated goat anti-rabbit IgG (1:10000) (Catalog: 111-055-144, RRID: AB_2337953, Jackson ImmunoResearch West Grove, PA) and stained using 1-Step NBT/BCIP solution (ThermoFisher).

RNA Isolation, Sequencing, Differential Gene Expression Analysis

To evaluate for transcriptomic differences between wild-type and BKO KPC cells, bulk RNA-seq was performed on 6 independent samples collected from each condition. Isolation was carried out as above and quality was tested for an RNA integrity number (RIN) > 7.5 on the Agilent 2100 bioanalyzer (Agilent

Technologies, Santa Clara, CA). A total of 300 ng of mRNA was enriched with poly-A selection and sequencing on the Illumina HiSeq2500 platform by the University of Wisconsin Biotechnology Sequencing Core. FASTq files were processed with Skewer and genes were filtered to remove those with low expression.[41] Samples were normalized by the method of trimmed mean of M-values.[42] Contrasts were drawn with the edgeR package, with differential expression taken when the FDR $q < 0.05$.[43] Pathway testing was performed with the KEGG database (Kyoto Encyclopedia of Genes and Genomes) using previously described methods.[44] The top 500 significant genes were inputted, ordered by q value, and the top 9 significant pathways (where $p < 0.05$) were plotted for visualization. Pathway dot size is indicative of the number of genes in each pathway. The RNA-seq data is publicly available through GEO (Accession number: GSE213680).

Heterotopic Tumor Modeling

To create flank tumors, 1 x 10^5 KPC or KPC-BKO cells were injected into the right flanks of immunocompetent C57BL/6J mice obtained from Jackson Laboratory (RRID: IMSR_JAX:000664, Bar Harbor, ME). Cells were mixed in a 1:1 50 μL solution of DMEM media and Matrigel (Corning Inc, Corning, NY). In the tumor growth experiment, a single dose of KPC or KPC-BKO cells was injected into C57BL/6J mice (male: n = 5, female: n = 5, each group) and tumors were measured twice weekly for four weeks starting on day 6 with the caliper method as previously described.[45] Tumor length and width were measured and tumor volume was calculated using the formula: tumor volume = length x width^2 x ½. Tumor weight was also measured (in mg) at the conclusion of the study period. Two independent replicate experiments were performed for tumors derived from KPC cells and KPC-BKO cells (total n = 20 mice per group). Additionally, two separate KPC-BKO clones were tested. Our power analysis, based on prior literature, indicated that using 10 mice per group would have 80% power to detect a 1.5-fold difference (alpha = 0.05) in tumor size (21 days after heterotopic injection) between KPC and KPC-BKO cells.[46] Mean differences between groups were computed using a t-test. In the tumor metastasis/survival experiment, the same dose of KPC or KPC-BKO cells was injected into C57BL/6J mice (n = 7 in each

group) and tumors were measured weekly until the mice became moribund or died. Kaplan Meier log-rank analysis was then performed to compare survival differences between conditions with the survival package.[47] A $p < 0.05$ is taken as significant for both experiments.

Cell cycle analysis

To evaluate the cell cycle of KPC and KPC-BKO cells, cells were grown to confluence, fixed with 70% ethanol, and stained with 50 μg/mL propidium iodide (Catalog: 421301, BioLegend, San Diego, CA) and 100 μg/mL RNAse A (Catalog: FEREN0531, Thermo Fisher). Samples (n = 3 technical replicates, each condition) were sorted with an Attune NxT flow cytometer (Thermo Fisher) and the DNA content was analyzed for the percent of cells in G1, S, and G2 phase with ModFit LT 6.0 software at the University of Wisconsin Carbone Cancer Center Flow Cytometry Laboratory. The average coefficient of variation (CV) of each sample was < 6%. Differences between conditions were tested with a t-test and a $p < 0.05$ was taken as statistically significant. This experiment was performed independently twice.

Chemotherapeutic Resistance Evaluation

To evaluate for chemotherapeutic resistance, KPC and KPC-BKO cells were grown in 96-well plates. Cells were washed and media containing either vehicle (DMSO, Catalog: D2650-100ML, MilliporeSigma) or increasing concentrations of gemcitabine (dose range = 10 nM to 1μM) (Catalog: G6423-50MG, MilliporeSigma) or paclitaxel (dose range = 10 nM to 1μM) (Catalog: AAJ62734MC, Thermo Fisher) was added to each well. Apoptosis was measured by detecting Caspase 3/7 activity after 24 hours of treatment using the Caspase-Glo 3/7 Assay System (Promega) on a BMG CLARIOstar plate reader. Dead-cell protease activity was similarly measured in cells after 20 hours of treatment using the CytoTox-Glo Cytotoxicity Assay (Promega) on a BMG CLARIOstar plate reader. Mean differences in the fold change between chemotherapy- and vehicle-treated cells were made with a t-test and a $p < 0.05$ was taken as statistically significant. Each experiment was completed with technical triplicates and independently replicated twice. A representative result is shown for each experiment.

Analysis

All analyses were performed in R version 4.2.0 or Julia version 0.3.12 unless otherwise indicated. Samples were not excluded from the analysis unless explicitly stated. Standard comparisons of the mean were performed with a t-test and survival was assessed with the log-rank test unless explicitly stated.

Results

The Clock in Human Pancreatic Ductal Adenocarcinoma is Less Robust Than in Normal Pancreatic Tissue

To test the hypothesis that the circadian clock is disrupted in human pancreatic ductal adenocarcinoma (PDAC), we used clock correlation, nCV, and CYCLOPS analysis on publicly available TCGA and CPTAC-3 pancreatic datasets (**Figure 1, Figure 2,** and **Figure 3**).[29,30] However, we first needed to ensure the validity of the pipeline in the pancreas since these had not been previously applied to pancreatic tissue. We assessed the clock in our existing murine normal circadian and chronic jetlag pancreas RNA-seq datasets by examining the clock correlation matrix and nCV.[23] These datasets contained pancreas samples acquired every 4 hours for 48 hours in male (n = 3 at each timepoint for each condition) and female (n = 3 at each timepoint for each condition) mice under standard lighting (normal circadian, n = 72) and chronic jetlag (n = 72) conditions. Chronic jetlag is known to affect the phase of gene expression but not the relative amplitude (rAMP) or the correlation of the core clock genes in the pancreas.[23] Correspondingly, we found that the core clock relationships remained intact on the correlation matrix when compared to the baseline clock correlation matrix for both normal and chronic jetlag conditions ($p < 0.001$, z-statistic = 54.96 vs. $p < 0.001$, z-statistic = 54.08) (**Supplemental Figure 1A**).[31,32] Further, the nCV of 11 clock genes remained unchanged ($p = 0.76$) between the normal circadian (mean nCV (± standard error) = 1.78 (± 0.27)) and chronic jetlag (mean nCV = 1.9 (± 0.28)) conditions (**Supplemental Figure 1B**) – consistent with the murine pancreatic clock being strongly rhythmic and intact, matching precisely what we had found in our prior longitudinal analysis.[23]

CYCLOPS was then used to reorder the mouse pancreas samples by their predicted phase, and cluster reordering of samples by CYCLOPS was analyzed for appropriate phase progression compared to the known zeitgeber time (ZT) of sample collection. Notably, CYCLOPS accurately (phase appropriately) reordered both the normal ($p < 0.01$; $\text{Met}^{\text{smooth}} = 0.90$) and the chronic jetlag conditions ($p < 0.01$; $\text{Met}^{\text{smooth}} = 0.97$), validating the pipeline for use in the pancreas (**Supplemental Figure 2B-C**). Collectively, these results confirmed the ability of nCV, correlation matrix, and CYCLOPS to determine the robustness of the circadian clock in the pancreas.

Considerable data support the tumor suppressor role of the circadian clock and the assertion that circadian disruption is present in human cancer.[48] In human PDAC, the supposition is that the clock may be altered, but supporting data is limited to the relative expression of single genes and is consequently inconclusive.[18,21,49] We therefore applied our pipeline to determine clock health in PDAC using the TCGA and CPTAC-3 pancreatic datasets.[22,26–30] After processing and batch correction of the 50 available normal and 318 available PDAC samples (**Supplemental Figure 3**), we examined the correlation matrix between the core clock genes (CCGs) and found that there was a weaker relationship amongst the CCGs in PDAC compared to normal (z-statistic PDAC = 13.77 vs. z-statistic normal = 22.42) (**Figure 1A**). Concordantly, we found that there was a clear decrease ($p = 0.04$) in the nCV between PDAC (mean nCV = 0.69 (± 0.08)) and normal (mean nCV = 1.03 (± 0.13)) (**Figure 1B**), indicating a weaker clock in PDAC compared to normal. We then applied our pancreatic CYCLOPS analysis (**Supplemental Figure 4**) which significantly reordered the normal samples ($p < 0.01$; $\text{Met}^{\text{smooth}} = 0.99$), indicating an intact clock. This was further reinforced when evaluating the predicted phase of CCGs and clock-controlled genes using CYCLOPS. We found that the phase sequence of normal pancreatic samples was similar to the phase sequence of mouse pancreatic samples (**Figure 2A-B**), with concordant phase in 12 out of 17 genes and ROR-phased genes largely peaking before E-box phase genes. Based on the CYCLOPS ordering, we analyzed the proportion of genes that were rhythmically expressed in normal pancreas. We found that 4,034/18,196 (22.17%) of normal pancreatic genes were rhythmic, (**Supplemental Data Files 2**). We

found that several key CCGs and clock-controlled genes were rhythmically expressed in normal samples on cosinor analysis, including *CLOCK*, *PER1*, *PER3*, *NR1D2*, *RORC*, *NFIL3*, *TEF*, *NR1D1*, *BHLHE40*, and *NPAS2* (**Figure 3A and Supplemental Table 1**). The CCGs *BMAL1* (p = 0.07, rAMP = 0.8) and *CRY1* (p = 0.08, rAMP = 0.48) were nearly rhythmic in the normal samples based on the pre-defined cutoff. Finally, phase set enrichment analysis (PSEA) was used to determine phase-dependent gene enrichment. The top 15 significant pathways were selected for analysis (**Figure 3C**). Consistent with our prior murine pancreas data, we found that normal pancreas was associated with time-dependent metabolic gene pathway enrichment.[23,50] In aggregate, this data confirms the health of the circadian clock in normal pancreatic tissue, which was expected but not previously shown.

Despite the validation steps and success in ordering normal pancreas, CYCLOPS could not reorder PDAC samples (p = 0.43; $\text{Met}^{\text{smooth}}$ = 0.99), revealing a less robust (or disrupted) clock in PDAC compared to normal. This inability to reorder strongly supports the attenuated circadian clock in PDAC identified with nCV and clock correlation analysis. We selected the best reordering available based on the eigengenes (**Supplemental Figure 4**) to enable visual representation of the PDAC samples compared to normal pancreas samples. This also enabled us to estimate as best as possible the rAMP of the PDAC samples (**Supplemental Data Files 3**), to coincide with the visual representation. Consistent with the nCV analysis, we found that rAMP decreased substantially in every core clock gene from normal to tumor (**Supplemental Table 1**), as evidenced by *PER1* and *PER3* expression (**Figure 3A**). Collectively, the weaker clock correlation, markedly reduced nCV, and CYCLOPS analysis of human population-level data convincingly show for the first time that the circadian clock is significantly disrupted in PDAC.

Creation of a Circadian Dysfunction Pancreatic Cancer Model

After demonstrating that the clock in human PDAC was dysfunctional, we sought to understand the potential clinical implications of clock disruption. Identifying an aberrant clock in other cancers has consistently demonstrated accelerated cancer progression and worse prognosis, while simultaneously revealing novel therapeutic targets.[15] Moreover, there appears to be a putative correlation between

suppressed *BMAL1* expression and poor prognosis in patients with PDAC.[17,18] Therefore, we hypothesized that disruption of the circadian clock in PDAC would cause accelerated cancer progression. To test this hypothesis, we used a syngeneic *Kras*- and *Trp53*-mutant pancreas cancer cell line (KPC) and employed CRISPR/Cas9 technology to functionally knockout *Bmal1* (KPC-BKO) so that we could examine the effects of clock dysfunction *in vitro* and *in vivo*.[37] The reason for mutating *Bmal1* in the PDAC cells was several-fold: i) KPC cells demonstrated an intact clock (see below) necessitating core clock gene modulation, ii) *BMAL1* is a central transcriptional regulator of the circadian clock machinery and suppressed gene expression has been found in several human cancers, correlating with worse prognosis,[13,15,17,18,20,21,51] iii) *BMAL1* expression is decreased in tumor compared to normal tissue in human PDAC,[18] iv) we similarly found a substantially dampened nCV (rAMP) of *BMAL1* expression in PDAC compared to normal tissue (*PER1*, *PER3*, *NR1D1*, and *BMAL1* displayed the greatest decrease in nCV), and v) segregating patients with PDAC into high and low *BMAL1* expression appears to be prognostic for survival outcomes.[17,18,21]

Consequently, guide RNAs were designed to target exon 8 of the *Bmal1* gene, which resulted in the insertion of adenine on one allele and a 2 base pair deletion on the other between nucleotide 81,074 and 81,075 at amino acid 73 (GRCm38) (**Figure 4A**). The result of both mutations was a frameshift just upstream of the basic helix loop helix (bHLH) domain known to assist the PAS A domain in heterodimerization with its binding partner CLOCK (**Figure 4B**).[52,53] Confirmatory western blotting revealed the presence of protein in wild-type (WT) cells and an absence of protein in *Bmal1* knockout (BKO) KPC cells (**Figure 4C**). To evaluate clock functionality, mRNA was isolated at 4-hour intervals (n = 3 per condition) for 24 hours after cell synchronization, and we performed RT-qPCR for *Per1*, a core downstream repressor of the positive arm of the molecular clock and a gene that demonstrated rhythmicity in our human normal CYCLOPS analysis (**Figure 4D**). Rhythmicity was assessed with the meta2d function of the Metacycle package.[34] KPC (WT) cells exhibited an intact and robust circadian clock with a $q = 0.0004$ and rAMP = 0.11 for *Per1*. To further evaluate the functionality of the clock in

KPC cells, luciferase activity driven by the *Per2* promoter was measured. Consistent with our evaluation of mRNA expression, luciferase activity in two separate clones was highly rhythmic (Clone 1: q = 5.51E-5, rAMP = 0.44; Clone 2: q = 1.95E-7, rAMP = 0.39) (**Supplemental Figure 5**). Conversely, KPC-BKO cells exhibited no detectable clock function with a q = 0.81 and rAMP = 0.003 for *Per1* expression (**Figure 4D)**. Consistent with the known cross-talk between the circadian clock and cell cycle, KPC-BKO cells demonstrated alterations in the cell cycle compared to KPC cells (**Figure 4E**).[20] BKO cells were found to have a higher mean (± standard error) percentage of cells in S phase (48.66 (± 0.13) vs. 36.96 (± 2.04); p = 0.029) and a lower percentage in G2 (18.03 (± 0.27) vs. 27.49 (± 0.89); p = 0.0053). There were no differences between KPC and KPC-BKO cells in G1 (35.56 (± 1.19) vs. 33.31 (± 0.17); p = 0.2). Taken together, these data demonstrate the successful creation of a novel PDAC cell line with an abolished clock (*Bmal1* gene mutation), which can be used to elucidate the repercussions of clock disruption in PDAC.

Clock Dysfunction Accelerates Pancreatic Cancer Growth

After establishing the model, we sought to understand how a dysfunctional clock impacted cell growth. KPC and KPC-BKO cells were grown in culture and injected into the right flanks of syngeneic C57BL/6J mice. Tumor growth was measured every 3-4 days for a total of 28 days to understand differences in primary tumor growth. We found that BKO caused an accelerated growth pattern, resulting in higher mean (± standard error) weight tumors at the study conclusion compared to KPC-derived tumors (438.02 ± 48.84 mg vs. 280.11 ± 42.73 mg; p = 0.02) (**Figure 5A-B**). These findings were evaluated and independently confirmed in a second identically created *Bmal1* mutant (functional knockout) clone (**Supplemental Figure 6**). Perhaps more relevant to human PDAC – given the aggressiveness of this cancer – we assessed the effect of clock disruption on survival (i.e. metastatic spread) by implanting KPC and KPC-BKO heterotopic tumors and observing the mice until moribund status or lethality (**Figure 5C**). Notably, the terminal endpoint occurred from metastatic spread to the diaphragm, lungs, or abdominal cavity, or uncommonly from locally advanced tumors. On Kaplan Meier log-rank analysis, mice

harboring tumors derived from KPC-BKO cells experienced worse survival than mice bearing KPC-derived tumors (median survival: 52 versus 75 days, $p = 0.04$). Thus, clock dysfunction resulted in accelerated tumor growth and earlier onset of tumor metastases (i.e., PDAC progression) *in vivo*, leading to worse overall survival.

Loss of Bmal1 Promotes the Enrichment of Cell Growth Pathways

To determine the possible etiologies of clock disruption causing accelerated PDAC progression, we compared the transcriptomic profiles of KPC and KPC-BKO cells. The principal component analysis revealed clear transcriptional profile differences between each condition (**Figure 6A**). Differential gene expression was quantified with edgeR and of the 15,110 genes, 5,235 (34.65%) were upregulated and 5,113 (33.84%) were downregulated in KPC-BKO compared to KPC cells (**Figure 6B, Supplemental Data File 4**).[43] When we examined the CCGs known to control the circadian cycle, we found that 12/15 examined clock genes were differentially expressed, including *Per1*, *Per2*, *Per3*, *Cry1*, *Cry2*, *Nr1d1*, *Nr1d2*, *Bhlhe40*, *Bhlhe41*, *Npas2*, *Arntl2*, and *Dbp* (All $q < 0.05$).[52] We then performed a KEGG pathway analysis to examine for enrichment of pathways as a result of *Bmal1* knockout in the PDAC cells (**Figure 5C**). We found that there was an enrichment of pathways important for cellular adhesion, such as ECM-Receptor Interaction, Cell Adhesion, and Focal Adhesion, as well as several cellular growth pathways including PI3K-AKT Signaling Pathway, MAPK Signaling Pathway, and Rap1 Signaling Pathway. Collectively, these data indicate that clock disruption in the KPC cells results in significant core clock gene changes and a transcriptional shift that alters key cancer promotion-related pathways such as cellular attachment and proliferation.

Cell Survival is Increased with the Loss of Bmal1 through Alterations in Multiple Cell Death Pathways

A hallmark of cancer progression is the inhibition of apoptosis.[54] This phenotype is readily apparent in response to chemotherapy. In particular, the mechanism of action of gemcitabine (inhibition of DNA synthesis) and paclitaxel (microtubule stabilization) – backbones in PDAC therapy – is to ultimately

induce apoptosis.[55,56] To understand the potential implications of clock disruption for PDAC patients undergoing treatment, we subjected KPC and KPC-BKO cells to 72 hours of chemotherapeutic treatment with either gemcitabine or paclitaxel.[57] We found that the activity of cell death pathways through apoptosis (measured by Caspase 3/7 activity) was blunted in response to both chemotherapeutic agents as a result of clock dysfunction (**Figure 7A**). We also assessed cytotoxic cell death, as measured by Dead-Cell Protease activity, and found that clock disruption promoted resistance to cytotoxic cell death induced by gemcitabine and paclitaxel (**Figure 7B**). Prior work has implicated alteration of Trp53 signaling to impact cell survival by suppressed apoptosis,[20] but KPC cells (both WT and BKO) are *Trp53* mutant ($Trp53^{R172H}$) indicating alternative mechanisms of heightened resistance in the KPC-BKO cells. Gemcitabine resistance in PDAC often occurs due to the downregulation of the channel protein hENT1 (*SLC29A1* gene), or deoxycytidine kinase (*DCK* gene) which activates gemcitabine once inside the cell.[58] However, these were only marginally downregulated (1.05-fold, $q = 0.04$ and 1.08-fold, $q = 0.02$) due to *Bmal1* knockout, and thus unlikely to contribute to the differences seen with clock disruption. Furthermore, these were non-rhythmic when examining our human samples, suggesting a lack of circadian control. Meanwhile, paclitaxel drug resistance is thought to occur mostly through upregulation of drug efflux transporter proteins (P-glycoprotein also known as multidrug-resistance associated protein), but these ATP-binding cassette transporter proteins (*Abcb1a and Abcb1b* genes) were instead significantly *downregulated* (8.2-fold, $q < 0.0001$ and 2.1-fold, $q < 0.0001$) in KPC-BKO vs KPC cells.[56] Concordantly, the *ABCB1* gene was rhythmic with elevated expression in the human normal samples ($p = 0.015$, rAMP = 0.95, mean expression = 73) compared to the human PDAC samples (mean expression = 23). Thus, the commonly described resistance mechanisms for gemcitabine and paclitaxel were not identified, underscoring the complexity of clock disruption induced chemotherapeutic resistance in cancer. Regardless, these data demonstrate that clock dysfunction promotes broad resistance in PDAC including multiple cell death pathways in the setting of two different PDAC backbone agents.

Discussion:

Our work herein used matched normal and tumor samples from TCGA and CPTAC-3 to provide the first substantive evidence that the circadian clock is disrupted in PDAC while the adjacent normal pancreatic clock is intact. To evaluate clock functionality in the pancreas, we assessed the clock with three complementary analyses not previously performed in pancreatic tissues: nCV, clock correlation, and CYCLOPS. The nCV was pioneered and validated in several tissues by Wu and colleagues.[25] It is a measurement that is directly related to the relative amplitude (rAMP) of the oscillation, and assesses overall and individual clock gene robustness.[25] For example, Wu and colleagues demonstrated that the nCV of core clock genes (CCGs) was consistently and significantly diminished in clock-disrupted tissues versus wild-type tissues (e.g. *Bmal1* knockout adipocytes vs wild-type adipocytes) and human datasets of tumor compared to matched (adjacent) normal tissue, where the timing of sample collection was unspecified.[25] It is therefore extraordinarily beneficial for understanding the rAMP of the circadian clock genes – a key measure of clock health – in population-level data where sample time acquisition is unknown. In conjunction with nCV, Shilts *et al*. developed the method of clock correlation to determine the progression of the clock in time-indeterminate datasets.[22] By capitalizing on the concept of co-expression of CCGs (intrinsic to the transcriptional translational feedback loop), Shilts and colleagues were able to computationally discern clock progression in transcriptomic data from numerous human datasets. Importantly, this technique is not dependent on full coverage of the period by samples, providing a beneficial approach for our normal data set which included only 50 samples and did not have phase representation across the 24-hour period. Furthermore, a direct comparison between heatmaps can be made (i.e. murine vs human or tumor vs normal) because each heatmap has the same corresponding color to rho correlation value.[22] Thus, when combining nCV and clock correlation analysis in unordered human samples, the health of the circadian clock in population-level data can be ascertained even when working with low sample numbers (at least 30).

Wu and colleagues applied nCV analysis to several paired tumor-normal datasets,[25] while Shilts *et al.* examined clock correlation in normal tissues and paired tumor-normal datasets.[22] However, we are the

first group to analyze the pancreas, possibly because our recent publication was the first to characterize the diurnal expression of mouse pancreatic genes over 48 hours.[23] Thus, an appropriate mouse reference group had not been published for comparison. In the study by Shilts *et al*., the human liver clock correlation heatmap (a similarly metabolic organ) demonstrated a weaker clock correlation versus the mouse reference, which they attributed to increased noise in the liver dataset.[22] Therefore, in our human data, we expected to identify an apparent 'diminished health' of the clock (lower nCV and weaker clock correlation) in the human pancreatic tissue versus mouse samples due to significant variation in the normal samples. This variability is contributed by human factors, such as type and timing of diet,[59,60] underlying genetic differences, and alterations in the 'normal pancreas' that surrounds the tumor (pancreatic atrophy, fibrosis, inflammation, etc.).[61] These can modulate the relative amplitude of oscillation or CCG correlation which contributes to significant noise in the data, as compared to the genetically identical, age-matched, and environmentally matched mouse samples.[22,28] Regardless of these limitations, the nCV and clock correlation revealed two key components of a healthy clock in human pancreas, which was an important component of the pipeline.

CYCLOPS is a machine learning method developed by Anafi *et al.*,[28] with subsequent elegant studies by Wu *et al*.,[26,27] to demonstrate how clock gene relationships can be used to infer and reorder samples by their predicted phase of expression to understand circadian biology in population-level data. The authors who developed CYCLOPS recommend roughly 250 samples for a complete phase distribution,[28] which is dependent on differences in time of surgery (presume specimens acquired between 6 AM and 6 PM) as well as differences in genetics and environmental factors (e.g. differences in sleep-wake cycle, or shift worker status).[62] CYCLOPS has been applied to the lung, liver, brain, hepatocellular carcinoma, and skin, but not the pancreas.[27,28] This is possibly due to known challenges associated with CYCLOPS, which includes optimizing the seed gene list for appropriate ordering.[28] We used the modified CYCLOPS approach by Wu *et al*. and were able to leverage our murine pancreatic longitudinal expression data to generate the seed gene list for use with human data, which increases the signal-to-noise ratio to optimize

ordering capability.[23,27,28] Thus, despite the expected variability in human normal pancreas samples, CYCLOPS significantly ordered the samples across the period, with several clock genes, including *CLOCK*, *PER1*, *PER3*, *NR1D2*, *RORC*, *NFIL3*, T*EF*, *NR1D1*, *BHLHE40*, and *NPAS2* demonstrating rhythmic expression. While *BMAL1* and *CRY1* did not pass our predetermined cutoff for rhythmicity in the normal samples, they demonstrated a robust rAMP with near-significant p values likely reflecting limitations with our sample number (i.e., distribution of samples across the period) than true lack of rhythmicity in the normal samples. As evidenced by the apparent gap in phase in the normal data, there was not uniform distribution of normal samples across the 24-hour period, which signifies a limitation of our analysis. However, despite these limitations, CYCLOPS statistically ordered the human normal data, and the phase-set enrichment analysis and predicted phase of expression (of most CCGs) aligned well with our prior mouse pancreas transcriptomic data (reference dataset). When combined with nCV and clock correlation, the data clearly demonstrate an intact clock in the human normal pancreas samples, which was an essential premise for evaluating the clock in human PDAC.

We then proceeded to use nCV, clock correlation, and CYCLOPS to provide compelling evidence of circadian clock disruption in PDAC. While the concept of circadian disruption in PDAC has been posited by others, past studies examining global clock function in human PDAC have been limited by detecting binary differences in overall RNA and protein expression between normal pancreas and PDAC.[17,18,20,21] Relles *et al.* found that several CCGs demonstrated decreased expression in PDAC compared to benign tumors or normal pancreas,[18] while Li *et al*. found that low *Bmal1* expression (compared to 'higher expression') was associated with worse disease-free and overall survival in patients with PDAC.[17] Similar studies have been repeated with concordant findings.[20,21] However, binary comparisons of expression are unlikely to capture the complexities of clock health such as rhythmicity, phase changes, changes in rAMP, or changes in clock progression. With the 318 available PDAC samples, we showed that there was markedly diminished nCV and a much weaker correlation among clock genes in PDAC compared to normal pancreas, depicting a loss of clock health in the cancer tissue. Further, although the inability to

reorder PDAC samples may be a limitation of CYCLOPS, it more likely indicates clock dysfunction.[63] In the PDAC samples, there was a sufficient sample number (n = 318) for phase distribution, but the rAMP of nearly all CCGs was markedly decreased (as visualized through best reordering), with many manifesting an arrhythmic pattern. Collectively, our approach to human data (nCV, clock correlation, and CYCLOPS) provided convincing evidence of clock disruption in PDAC.

The main limitation of our current strategy is the inability to discern why there was a loss of circadian signatures in human PDAC population data. These observations could be the consequence of i) dampening of the clock to a significant extent in every patient (i.e., global phenomena), ii) differences in the extent to which the clock is disrupted (i.e., substantial clock dysfunction in a certain subset of patients), or iii) biological heterogeneity in the PDAC samples surpassing circadian variability. The last consideration seems unlikely given the marked decrease in rAMP (nCV) and clock correlation showing significantly diminished clock health in PDAC. Furthermore, as seen with the CYCLOPS ordered *PER1* expression data over the 24-hr period (Figure 3A), enhanced variability did not lead to the apparent arrhythmicity in PDAC. Unfortunately, we were unable to discriminate between the first two possibilities. The literature in cancer would suggest that cohorts of patients exhibit a differential extent of clock disruption in their tumors (i.e. some clock intact vs some markedly disrupted),[15,17,18,51] which would result in an overall loss of circadian signatures seen in the nCV, clock correlation, and CYCLOPS analysis. Our assessment of clock function in the KPC cells would also support this hypothesis, given that the clock was intact in the *Kras*- and *Trp53*-mutant pancreas cancer cells and necessitated *Bmal1* mutagenesis to generate clock disruption. Further, we assessed the cycling of the *Per1* gene and *Per2*-luciferase in the KPC cells and identified a robust rhythm; by comparison, the human PDAC samples demonstrated arrhythmic *PER1* expression. Therefore, we generated the novel murine KPC-BKO cell line as a basis to evaluate clock disruption in PDAC, and intend for this cell line to be a useful approach for investigators evaluating the clock in PDAC.

Using our KPC and KPC-BKO cells, we found accelerated tumor growth in our syngeneic *in vivo* model with *Bmal1* functional knockout. Our preference was to use an immune-competent model given the known impact of the circadian clock on the immune system (another strength of our model).[64,65] Interestingly, our primary tumor growth results were similar to results by Jiang and colleagues, who used implanted human PDAC cells (BxPC-3 and PANC-1) into immunocompromised mice after shRNA knockdown of *Bmal1*.[20,21] However, patients with PDAC ultimately succumb to distant metastatic spread, rather than local tumor growth, and so examining the contribution of clock disruption to overall survival was of greater importance.[66] We found that *Bmal1* mutation promoted earlier metastatic spread of tumors resulting in earlier lethality, which has not been shown before. Concordant with the aggressive tumor phenotype, *Bmal1* mutation also caused resistance to chemotherapy. While resistance to gemcitabine has been shown,[21] we found chemoresistance to two different backbone anti-cancer agents (gemcitabine and paclitaxel), including suppressed apoptosis and cytotoxicity, indicating a more broad resistance to standard PDAC chemotherapy. Although suppressed *Bmal1* expression in PDAC has been suggested to modulate *Trp53* to promote a tumor suppressor effect, this was unlikely the case in our study considering KPC cells are a *Trp53*-mutant cell line.[20] Other work indicates the transcription factor YY1 is significantly overexpressed in PDAC and ultimately causes BMAL1 suppression with consequent PDAC progression and resistance to gemcitabine (unclear mechanism of resistance).[21] Yet, when we examined our human PDAC and human normal samples, we found that *YY1* expression was equivalent between the groups (mean expression 101.61 versus 102.87). Turning to other cancers where BMAL1 is suppressed, *MYC* amplification in neuroblastoma alters *BMAL1* mRNA expression through induction of *NR1D1*.[51,67] Notably, this is associated with poor prognosis and is *BMAL1* dependent since ectopic expression of *BMAL1* inhibits tumor growth. This mechanism is unlikely to be occurring in PDAC since there is no upregulation of *MYC*, *MYC-N*, or *NR1D1* gene expression in human PDAC compared to normal samples. While common resistance mechanisms of gemcitabine and paclitaxel were not reflected in the human PDAC versus human normal data or the KPC versus KPC-BKO cells (e.g. channel proteins), RNA sequencing identified several enriched pathways integral to cancer progression and chemoresistance in the

Bmal1 functional knockout cells, such as the PI3K-AKT pathway.[68,69] The PI3K-AKT pathway is inextricably linked to cancer cell proliferation and resistance to apoptosis, indicating a plausible mechanism for inhibition of programmed cell death to multiple agents seen in our study.[70,71] Further, resistance to paclitaxel is associated with the activation of the PI3K-AKT pathway,[72] and similar correlations have been identified with gemcitabine resistance.[73,74] However, the mechanism of chemoresistance is quite complex and the etiology for suppressed apoptosis and cytotoxicity due to clock disruption remains unclear. In future work, we can employ a series of clock-manipulated PDAC cell lines to better understand the contributions of clock disruption to chemoresistance and PDAC progression.

In conclusion, we used a comprehensive approach (nCV, clock correlation, and CYCLOPS) to evaluate the health of the circadian clock in human normal pancreas and demonstrated clock disruption in human PDAC. Additionally, we developed novel cell lines to evaluate the repercussions of clock disruption in PDAC and identified factors associated with poor prognosis (i.e., earlier metastases, resistance to chemotherapy, and enrichment of cancer-related pathways). Future work will expand on this foundation to disentangle the clock-dependent effects of PDAC and consequently focus therapeutic efforts.

Acknowledgments:

We would like to acknowledge the Gene Expression Center and the Bioinformatics Resource Center (BRC) at the University of Wisconsin, Madison for their contributions to this work. The authors thank the University of Wisconsin Carbone Cancer Center Flow Cytometry Laboratory, supported by P30 CA014520, for use of its facilities and services. We would also like to thank the Michael W. Oglesby Foundation for their funding support of our work in circadian disruption and pancreas pathology.

Materials Availability Statement:

The modified KPC cell lines (KPC-BKO and KPC Per2-dLuc) created for use in this manuscript are available upon reasonable request from the corresponding author, Sean Ronnekleiv-Kelly.

Data Availability Statement:

The TCGA and CPTAC-3 data were requested from the following URL: https://portal.gdc.cancer.gov/. All RNAseq data can be found on the Gene Expression Omnibus (GEO) at accession numbers GSE213680 and GSE165198.

References

1. Bass J, Lazar MA. Circadian time signatures of fitness and disease. *Science*. 2016;354(6315):994-999. doi:10.1126/science.aah4965

2. Aryal RP, Kwak PB, Tamayo AG, et al. Macromolecular Assemblies of the Mammalian Circadian Clock. *Mol Cell*. 2017;67(5):770-782.e6. doi:10.1016/j.molcel.2017.07.017

3. Transcriptional architecture of the mammalian circadian clock - PubMed. Accessed October 10, 2022. https://pubmed.ncbi.nlm.nih.gov/27990019/

4. Allada R, Bass J. Circadian Mechanisms in Medicine. *N Engl J Med*. 2021;384(6):550-561. doi:10.1056/NEJMra1802337

5. Fishbein AB, Knutson KL, Zee PC. Circadian disruption and human health. *J Clin Invest*. 2021;131(19):e148286. doi:10.1172/JCI148286

6. West AC, Smith L, Ray DW, Loudon ASI, Brown TM, Bechtold DA. Misalignment with the external light environment drives metabolic and cardiac dysfunction. *Nat Commun*. 2017;8(1):417. doi:10.1038/s41467-017-00462-2

7. Marcheva B, Ramsey KM, Buhr ED, et al. Disruption of the clock components CLOCK and BMAL1 leads to hypoinsulinaemia and diabetes. *Nature*. 2010;466(7306):627-631. doi:10.1038/nature09253

8. Roenneberg T, Allebrandt KV, Merrow M, Vetter C. Social jetlag and obesity. *Curr Biol CB*. 2012;22(10):939-943. doi:10.1016/j.cub.2012.03.038

9. Parsons MJ, Moffitt TE, Gregory AM, et al. Social jetlag, obesity and metabolic disorder: investigation in a cohort study. *Int J Obes 2005*. 2015;39(5):842-848. doi:10.1038/ijo.2014.201

10. Knutson KL, Wu D, Patel SR, et al. Association Between Sleep Timing, Obesity, Diabetes: The Hispanic Community Health Study/Study of Latinos (HCHS/SOL) Cohort Study. *Sleep*. 2017;40(4). doi:10.1093/sleep/zsx014

11. Turek FW, Joshu C, Kohsaka A, et al. Obesity and metabolic syndrome in circadian Clock mutant mice. *Science*. 2005;308(5724):1043-1045. doi:10.1126/science.1108750

12. Dong Z, Zhang G, Qu M, et al. Targeting Glioblastoma Stem Cells through Disruption of the Circadian Clock. *Cancer Discov*. 2019;9(11):1556-1573. doi:10.1158/2159-8290.CD-19-0215

13. Papagiannakopoulos T, Bauer MR, Davidson SM, et al. Circadian Rhythm Disruption Promotes Lung Tumorigenesis. *Cell Metab*. 2016;24(2):324-331. doi:10.1016/j.cmet.2016.07.001

14. Kettner NM, Voicu H, Finegold MJ, et al. Circadian Homeostasis of Liver Metabolism Suppresses Hepatocarcinogenesis. *Cancer Cell*. 2016;30(6):909-924. doi:10.1016/j.ccell.2016.10.007

15. Moreno-Smith M, Milazzo G, Tao L, et al. Restoration of the molecular clock is tumor suppressive in neuroblastoma. *Nat Commun*. 2021;12(1):4006. doi:10.1038/s41467-021-24196-4

16. Sulli G, Rommel A, Wang X, et al. Pharmacological activation of REV-ERBs is lethal in cancer and oncogene induced senescence. *Nature*. 2018;553(7688):351-355. doi:10.1038/nature25170

17. Li W, Liu L, Liu D, et al. Decreased circadian component Bmal1 predicts tumor progression and poor prognosis in human pancreatic ductal adenocarcinoma. *Biochem Biophys Res Commun*. 2016;472(1):156-162. doi:10.1016/j.bbrc.2016.02.087

18. Relles D, Sendecki J, Chipitsyna G, Hyslop T, Yeo CJ, Arafat HA. Circadian gene expression and clinicopathologic correlates in pancreatic cancer. *J Gastrointest Surg Off J Soc Surg Aliment Tract*. 2013;17(3):443-450. doi:10.1007/s11605-012-2112-2

19. Siegel RL, Miller KD, Fuchs HE, Jemal A. Cancer statistics, 2022. *CA Cancer J Clin*. 2022;72(1):7-33. doi:10.3322/caac.21708

20. Jiang W, Zhao S, Jiang X, et al. The circadian clock gene Bmal1 acts as a potential anti-oncogene in pancreatic cancer by activating the p53 tumor suppressor pathway. *Cancer Lett*. 2016;371(2):314-325. doi:10.1016/j.canlet.2015.12.002

21. Jiang W, Zhao S, Shen J, et al. The MiR-135b-BMAL1-YY1 loop disturbs pancreatic clockwork to promote tumourigenesis and chemoresistance. *Cell Death Dis*. 2018;9(2):149. doi:10.1038/s41419-017-0233-y

22. Shilts J, Chen G, Hughey JJ. Evidence for widespread dysregulation of circadian clock progression in human cancer. *PeerJ*. 2018;6:e4327. doi:10.7717/peerj.4327

23. Schwartz PB, Walcheck MT, Berres ME, et al. Chronic Jetlag-Induced Alterations in Pancreatic Diurnal Gene Expression. *Physiol Genomics*. Published online May 31, 2021. doi:10.1152/physiolgenomics.00022.2021

24. Hughes ME, Abruzzi KC, Allada R, et al. Guidelines for Genome-Scale Analysis of Biological Rhythms. *J Biol Rhythms*. 2017;32(5):380-393. doi:10.1177/0748730417728663

25. Wu G, Francey LJ, Ruben MD, Hogenesch JB. Normalized coefficient of variation (nCV): a method to evaluate circadian clock robustness in population scale data. *Bioinformatics*. 2021;37(23):4581-4583. doi:10.1093/bioinformatics/btab731

26. Wu G, Ruben MD, Francey LJ, et al. A population-based gene expression signature of molecular clock phase from a single epidermal sample. *Genome Med*. 2020;12(1):73. doi:10.1186/s13073-020-00768-9

27. Wu G, Ruben MD, Schmidt RE, et al. Population-level rhythms in human skin with implications for circadian medicine. *Proc Natl Acad Sci U S A*. 2018;115(48):12313-12318. doi:10.1073/pnas.1809442115

28. Anafi RC, Francey LJ, Hogenesch JB, Kim J. CYCLOPS reveals human transcriptional rhythms in health and disease. *Proc Natl Acad Sci U S A*. 2017;114(20):5312-5317. doi:10.1073/pnas.1619320114

29. Edwards NJ, Oberti M, Thangudu RR, et al. The CPTAC Data Portal: A Resource for Cancer Proteomics Research. *J Proteome Res*. 2015;14(6):2707-2713. doi:10.1021/pr501254j

30. Cancer Genome Atlas Research Network, Weinstein JN, Collisson EA, et al. The Cancer Genome Atlas Pan-Cancer analysis project. *Nat Genet*. 2013;45(10):1113-1120. doi:10.1038/ng.2764

31. Pizarro A, Hayer K, Lahens NF, Hogenesch JB. CircaDB: a database of mammalian circadian gene expression profiles. *Nucleic Acids Res*. 2013;41(Database issue):D1009-1013. doi:10.1093/nar/gks1161

32. Zhang R, Lahens NF, Ballance HI, Hughes ME, Hogenesch JB. A circadian gene expression atlas in mammals: Implications for biology and medicine. *Proc Natl Acad Sci*. 2014;111(45):16219-16224. doi:10.1073/pnas.1408886111

33. Leng N, Chu LF, Barry C, et al. Oscope identifies oscillatory genes in unsynchronized single cell RNA-seq experiments. *Nat Methods*. 2015;12(10):947-950. doi:10.1038/nmeth.3549

34. Wu G, Anafi RC, Hughes ME, Kornacker K, Hogenesch JB. MetaCycle: an integrated R package to evaluate periodicity in large scale data. *Bioinforma Oxf Engl*. 2016;32(21):3351-3353. doi:10.1093/bioinformatics/btw405

35. Leek JT, Johnson WE, Parker HS, Jaffe AE, Storey JD. The sva package for removing batch effects and other unwanted variation in high-throughput experiments. *Bioinforma Oxf Engl*. 2012;28(6):882-883. doi:10.1093/bioinformatics/bts034

36. Zhang R, Podtelezhnikov AA, Hogenesch JB, Anafi RC. Discovering Biology in Periodic Data through Phase Set Enrichment Analysis (PSEA). *J Biol Rhythms*. 2016;31(3):244-257. doi:10.1177/0748730416631895

37. Hingorani SR, Wang L, Multani AS, et al. Trp53R172H and KrasG12D cooperate to promote chromosomal instability and widely metastatic pancreatic ductal adenocarcinoma in mice. *Cancer Cell*. 2005;7(5):469-483. doi:10.1016/j.ccr.2005.04.023

38. Clement K, Rees H, Canver MC, et al. CRISPResso2 provides accurate and rapid genome editing sequence analysis. *Nat Biotechnol*. 2019;37(3):224-226. doi:10.1038/s41587-019-0032-3

39. Mei L, Fan Y, Lv X, Welsh DK, Zhan C, Zhang EE. Long-term in vivo recording of circadian rhythms in brains of freely moving mice. *Proc Natl Acad Sci U S A*. 2018;115(16):4276-4281. doi:10.1073/pnas.1717735115

40. Ramanathan C, Khan SK, Kathale ND, Xu H, Liu AC. Monitoring Cell-autonomous Circadian Clock Rhythms of Gene Expression Using Luciferase Bioluminescence Reporters. *J Vis Exp JoVE*. 2012;(67):4234. doi:10.3791/4234

41. Jiang H, Lei R, Ding SW, Zhu S. Skewer: a fast and accurate adapter trimmer for next-generation sequencing paired-end reads. *BMC Bioinformatics*. 2014;15:182. doi:10.1186/1471-2105-15-182

42. Robinson MD, Oshlack A. A scaling normalization method for differential expression analysis of RNA-seq data. *Genome Biol*. 2010;11(3):R25. doi:10.1186/gb-2010-11-3-r25

43. Robinson MD, McCarthy DJ, Smyth GK. edgeR: a Bioconductor package for differential expression analysis of digital gene expression data. *Bioinforma Oxf Engl*. 2010;26(1):139-140. doi:10.1093/bioinformatics/btp616

44. clusterProfiler: an R Package for Comparing Biological Themes Among Gene Clusters | OMICS: A Journal of Integrative Biology. Accessed August 28, 2022. https://www.liebertpub.com/doi/10.1089/omi.2011.0118

45. Euhus DM, Hudd C, Laregina MC, Johnson FE. Tumor measurement in the nude mouse. *J Surg Oncol*. 1986;31(4):229-234. doi:10.1002/jso.2930310402

46. Alexander RK, Liou YH, Knudsen NH, et al. Bmal1 integrates mitochondrial metabolism and macrophage activation. *eLife*. 2020;9:e54090. doi:10.7554/eLife.54090

47. Therneau T. A Package for Survival Analysis in R. https://CRAN.R-project.org/package=survival

48. Fu L, Kettner NM. The circadian clock in cancer development and therapy. *Prog Mol Biol Transl Sci*. 2013;119:221-282. doi:10.1016/B978-0-12-396971-2.00009-9

49. Pogue-Geile KL, Lyons-Weiler J, Whitcomb DC. Molecular overlap of fly circadian rhythms and human pancreatic cancer. *Cancer Lett*. 2006;243(1):55-57. doi:10.1016/j.canlet.2005.11.049

50. Schwartz PB, Barrett-Wilt GA, Ronnekleiv-Kelly SM. Chronic Jetlag Alters the Landscape of the Pancreatic Lipidome. *Pancreas*. 2022;51(1):80-89. doi:10.1097/MPA.0000000000001962

51. Altman BJ, Hsieh AL, Sengupta A, et al. MYC Disrupts the Circadian Clock and Metabolism in Cancer Cells. *Cell Metab*. 2015;22(6):1009-1019. doi:10.1016/j.cmet.2015.09.003

52. McIntosh BE, Hogenesch JB, Bradfield CA. Mammalian Per-Arnt-Sim proteins in environmental adaptation. *Annu Rev Physiol*. 2010;72:625-645. doi:10.1146/annurev-physiol-021909-135922

53. Vazquez-Rivera E, Rojas B, Parrott JC, et al. The aryl hydrocarbon receptor as a model PAS sensor. *Toxicol Rep*. 2022;9:1-11. doi:10.1016/j.toxrep.2021.11.017

54. Evan GI, Vousden KH. Proliferation, cell cycle and apoptosis in cancer. *Nature*. 2001;411(6835):342-348. doi:10.1038/35077213

55. Mini E, Nobili S, Caciagli B, Landini I, Mazzei T. Cellular pharmacology of gemcitabine. *Ann Oncol Off J Eur Soc Med Oncol*. 2006;17 Suppl 5:v7-12. doi:10.1093/annonc/mdj941

56. Kampan NC, Madondo MT, McNally OM, Quinn M, Plebanski M. Paclitaxel and Its Evolving Role in the Management of Ovarian Cancer. *BioMed Res Int*. 2015;2015:413076. doi:10.1155/2015/413076

57. Goldstein D, El-Maraghi RH, Hammel P, et al. nab-Paclitaxel plus gemcitabine for metastatic pancreatic cancer: long-term survival from a phase III trial. *J Natl Cancer Inst*. 2015;107(2). doi:10.1093/jnci/dju413

58. de Sousa Cavalcante L, Monteiro G. Gemcitabine: metabolism and molecular mechanisms of action, sensitivity and chemoresistance in pancreatic cancer. *Eur J Pharmacol*. 2014;741:8-16. doi:10.1016/j.ejphar.2014.07.041

59. Brown MR, Matveyenko AV. It’s What and When You Eat: An Overview of Transcriptional and Epigenetic Responses to Dietary Perturbations in Pancreatic Islets. *Front Endocrinol*. 2022;13:842603. doi:10.3389/fendo.2022.842603

60. Fadista J, Vikman P, Laakso EO, et al. Global genomic and transcriptomic analysis of human pancreatic islets reveals novel genes influencing glucose metabolism. *Proc Natl Acad Sci U S A*. 2014;111(38):13924-13929. doi:10.1073/pnas.1402665111

61. Korpela T, Ristimäki A, Udd M, et al. Pancreatic fibrosis, acinar atrophy and chronic inflammation in surgical specimens associated with survival in patients with resectable pancreatic ductal adenocarcinoma. *BMC Cancer*. 2022;22(1):23. doi:10.1186/s12885-021-09080-0

62. Archer SN, Laing EE, Möller-Levet CS, et al. Mistimed sleep disrupts circadian regulation of the human transcriptome. *Proc Natl Acad Sci U S A*. 2014;111(6):E682-E691. doi:10.1073/pnas.1316335111

63. Wu G, Ruben MD, Francey LJ, Lee YY, Anafi RC, Hogenesch JB. An in silico genome-wide screen for circadian clock strength in human samples. Published online May 25, 2022:2022.05.10.491250. doi:10.1101/2022.05.10.491250

64. Yu X, Rollins D, Ruhn KA, et al. TH17 cell differentiation is regulated by the circadian clock. *Science*. 2013;342(6159):727-730. doi:10.1126/science.1243884

65. Druzd D, Matveeva O, Ince L, et al. Lymphocyte Circadian Clocks Control Lymph Node Trafficking and Adaptive Immune Responses. *Immunity*. 2017;46(1):120-132. doi:10.1016/j.immuni.2016.12.011

66. Conroy T, Hammel P, Hebbar M, et al. FOLFIRINOX or Gemcitabine as Adjuvant Therapy for Pancreatic Cancer. *N Engl J Med*. 2018;379(25):2395-2406. doi:10.1056/NEJMoa1809775

67. Altman BJ, Hsieh AL, Gouw AM, Dang CV. Correspondence: Oncogenic MYC persistently upregulates the molecular clock component REV-ERBα. *Nat Commun*. 2017;8:14862. doi:10.1038/ncomms14862

68. Murthy D, Attri KS, Singh PK. Phosphoinositide 3-Kinase Signaling Pathway in Pancreatic Ductal Adenocarcinoma Progression, Pathogenesis, and Therapeutics. *Front Physiol*. 2018;9:335. doi:10.3389/fphys.2018.00335

69. Bryant KL, Stalnecker CA, Zeitouni D, et al. Combination of ERK and autophagy inhibition as a treatment approach for pancreatic cancer. *Nat Med*. 2019;25(4):628-640. doi:10.1038/s41591-019-0368-8

70. Hoxhaj G, Manning BD. The PI3K-AKT network at the interface of oncogenic signalling and cancer metabolism. *Nat Rev Cancer*. 2020;20(2):74-88. doi:10.1038/s41568-019-0216-7

71. Mortazavi M, Moosavi F, Martini M, Giovannetti E, Firuzi O. Prospects of targeting PI3K/AKT/mTOR pathway in pancreatic cancer. *Crit Rev Oncol Hematol*. 2022;176:103749. doi:10.1016/j.critrevonc.2022.103749

72. Maloney SM, Hoover CA, Morejon-Lasso LV, Prosperi JR. Mechanisms of Taxane Resistance. *Cancers*. 2020;12(11):E3323. doi:10.3390/cancers12113323

73. Yang XL, Lin FJ, Guo YJ, Shao ZM, Ou ZL. Gemcitabine resistance in breast cancer cells regulated by PI3K/AKT-mediated cellular proliferation exerts negative feedback via the MEK/MAPK and mTOR pathways. *OncoTargets Ther*. 2014;7:1033-1042. doi:10.2147/OTT.S63145

74. Li W, Zhu Y, Zhang K, et al. PROM2 promotes gemcitabine chemoresistance via activating the Akt signaling pathway in pancreatic cancer. *Exp Mol Med*. 2020;52(3):409-422. doi:10.1038/s12276-020-0390-4

Figures:

Figure 1: *The human pancreatic clock robustness is diminished after malignant transformation.* **A**. Clock correlation matrices were created for normal (left; n = 50) and pancreatic ductal adenocarcinoma (right; n

= 318) samples. **B**. The normalized coefficient of variation (nCV) was calculated to determine the robustness of the pancreatic clock for the normal (circles) and PDAC (triangles) samples. Each color indicates a different gene evaluated.

Figure 2: *Clock phase predictions demonstrate conserved clock relationships*: **A.** Graphical representation and **B.** table of the CCG and clock-controlled gene phase prediction from the cosinor analysis of CYCLOPS reordered human pancreas samples (n = 50) and Metacycle predicted phases of mouse pancreas samples (n = 72), relative to *BMAL1* (human) and *Bmal1* (mouse) phase.

Figure 3: *The human pancreatic cancer tumor clock is dysfunctional relative to the normal pancreas.* **A**. CYCLOPS was used to reorder samples from normal (n = 50) and pancreatic ductal adenocarcinoma (n = 318) TCGA and CPTAC-3 samples. Plots from several core clock genes reordered by CYCLOPS in normal tissue as compared to best reordering in PDAC (**A**) are shown – ordered from 0 to 2π. Shading around the blue regression line indicates the 95% confidence interval. **B**. Graphical representation of Phase Set Enrichment Analysis (PSEA) of normal pancreatic samples, ordered by phase of expression.

Figure 4: *Creation of a mouse clock dysfunction cell line model.* **A**. The core clock gene *Bmal1* was mutated (functional knockout) in KPC murine pancreatic cells with CRISPR-Cas9 genome editing technology (BKO) with the frameshift site indicated by the blue line. **B.** The frameshift mutation was induced upstream of the basic helix loop helix (bHLH) domain (red star). The resulting protein lacked critical downstream elements for functionality, including the PAS-A, PAS-B, and PAC domains. **C.** Western blot demonstrating the loss of BMAL1 protein across 24 hours for wild-type (WT) and BKO cells (M = marker lane). **D.** The mean (± standard error) *Per1* mRNA expression of synchronized KPC (n = 3 at each time point; black dashed) and KPC-BKO (n = 3 at each time point; grey) cells from ZT0-ZT24. **E.** Graphs comparing the percent of cells in G1, S, and G2 in WT (n = 3; white) and BKO (n = 3; grey) KPC cells.

Figure 5: *Mutation of Bmal1 promotes pancreatic cancer progression.* **A.**Comparison of mouse tumor weight at 28 days for WT (n = 20; white) and BKO (n = 20) KPC tumors.**B.** WT (n = 20; black) and BKO (n = 20) mean (± standard error) tumor size (in mm^3) over the 28-day growth period. **C.** Kaplan Meier survival curve for mice implanted with WT (n = 7; black) and BKO (n =7; grey) KPC tumors. The dotted lines indicate the median survival. [ns = not significant, * = $p < 0.05$, ** = $p < 0.01$]

Figure 6: *Functional knockout of Bmal1 promotes widespread transcriptomic alterations and activation of multiple oncogenic pathways.* **A.** Principal Component Analysis (PCA) demonstrating overall differences in expression between WT(green) and BKO (purple) samples (n = 6 each) **B.** Volcano plot showing genes that were significantly upregulated (red) and downregulated (blue) on differential gene expression (DGE) analysis ($q < 0.05$). All significant core clock genes are highlighted **C.** KEGG analysis was then performed, and the top 9 pathways ordered by significance are shown. For each pathway, the size of each dot corresponds to the number of genes involved in each pathway.

Figure 7: *Clock dysfunction diminishes the chemotherapeutic cell death response.* KPC wildtype (WT) and KPC-BKO cells (n = 3) were treated with increasing doses of gemcitabine and paclitaxel. Fold change differences (± standard error) in Caspase 3/7 activity in response to either **A.** gemcitabine or **B.** paclitaxel. Fold change differences (± standard error) in dead-cell protease activity in response to **C.** gemcitabine or **D.** paclitaxel. [ns = not significant, * = $p < 0.05$, ** = $p < 0.01$, *** = $p < 0.001$]

<u>Supplementary Files:</u>

Supplementary Data Files:

Supplemental Data File 1: CYCLOPS seed gene list.

Supplemental Data File 2: Significant genes on cosinor analysis for normal CYCLOPS reordered normal pancreas

Supplemental Data File 3: Significant genes on cosinor analysis for normal CYCLOPS reordered PDAC

Supplemental Data File 4: KPC wildtype versus BKO edgeR differential gene expression

Supplementary Figures:

Supplemental Figure 1: *The wildtype mouse pancreatic clock is intact and robust.* **A**. Clock correlation matrices were created for normal (left, n = 72) and pancreatic ductal adenocarcinoma (right, n = 72) samples. **B**. The normalized coefficient of variation (nCV) was calculated to determine the robustness of the pancreatic clock for the normal circadian (circles) and chronic jetlag (triangles) pancreas samples. Each color indicates a different gene evaluated.

Supplemental Figure 2: *CYCLOPS accurately reorders wildtype mouse pancreas samples.* Eigengenes identified by Oscope for use in CYCLOPS in **A.** normal circadian (upper) and chronic jetlag (lower) samples. Shading around the blue regression line indicates the 95% confidence interval for each plot. **B.** The normal circadian (left) and chronic jetlag (right) clusters ordered by CYCLOPS demonstrate accurate reordering for both conditions **C.** Normal circadian (left) and chronic jetlag (right) genes found to be significantly rhythmic on both CYCLOPS reordered cosinor analysis and rhythmicity testing based on the known sample collection time with the Metacycle meta3d function are ordered by their predicted phase of expression. Clock genes are shown in orange.

Supplemental Figure 3: *Normal pancreatic and pancreatic ductal adenocarcinoma (PDAC) samples were processed and filtered.* TCGA and CPTAC-3 samples were processed and batched corrected. An MDS plot is shown demonstrating differences between the matched normal (green; n = 50) and PDAC (purple; n = 318) samples.

Supplemental Figure 4: *Eigengenes for the human normal pancreas and pancreatic ductal adenocarcinoma (PDAC) samples.* Eigengenes were selected by Oscope for normal (upper) and PDAC (lower) samples for use in CYCLOPS. Shading around the blue regression line indicates the 95% confidence interval for each plot.

Supplemental Figure 5: *KPC cells expressing dLuciferase driven by the Per2 promoter exhibit circadian activity.* Two independent clones were examined, and luciferase activity was measured at 4-hour intervals. Rhythmicity was calculated with Metacycle. Clone 1 (left) was found to be rhythmic with a q = 5.51E-5 and rAMP = 0.44. Clone 2 (right) was found to be rhythmic with a q = 1.95E-7, rAMP = 0.39.

Supplemental Figure 6: *Cross-validation of mutant Bmal1 (functional knockout) growth in a second independent clone.* A second independent *Bmal1* knockout (BKO) clone with an identical mutation to the first was validated with **A.** western blot analysis. We then heterotopically implanted wildtype (WT) and BKO cells into C57BL/6J mice and followed **B.** tumor weight and **C.** cell growth. BKO_2 (dark grey; n = 20) had a similar mean (± standard error) tumor weight to BKO_1 (light grey; n = 20) (426.09 (± 40.07) mg vs 438.02 (± 48.84) mg; p = 0.85), and both BKO_2 (426.09 (± 40.07) mg vs 280.11 (± 42.73) mg; p = 0.017) and BKO_1 (438.02 (± 48.84) mg vs 280.11 (± 42.73) mg; p = 0.02) were larger than WT (white; n = 20). BKO_1 and BKO_2 had similar significantly faster growth trajectories. [ns = not significant, * = p < 0.05, ** = p < 0.01, *** = p < 0.001]

Supplementary Tables

Supplemental Table 1: Cosinor rhythmicity analysis of CYCLOPS ordered normal pancreas and PDAC

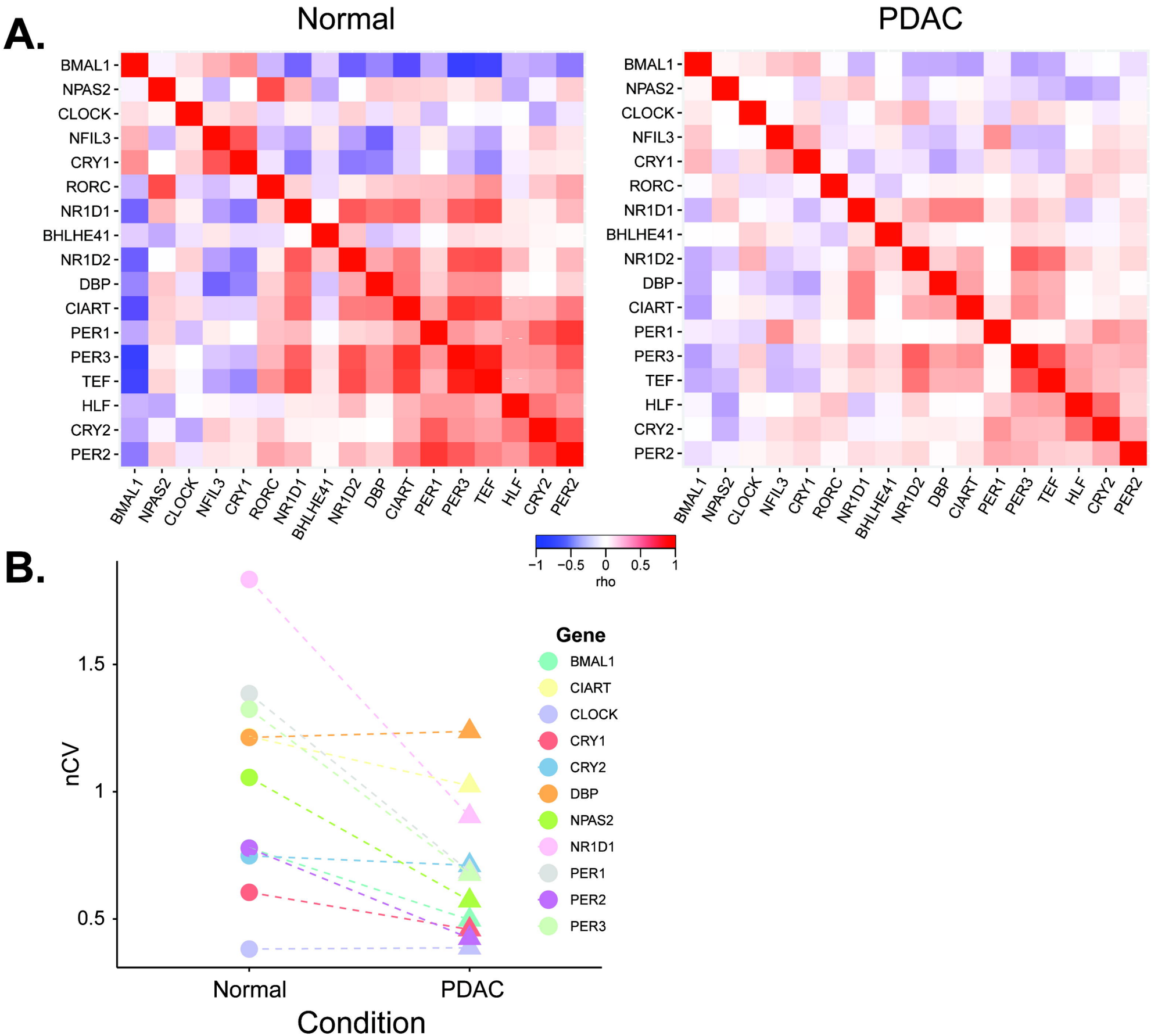
A.
Normal
PDAC
BMAL1
NPAS2
CLOCK
NFIL3
CRY1
RORC
NR1D1
BHLHE41
NR1D2
DBP
CIART
PER1
PER3
TEF
HLF
CRY2
PER2
−1
−0.5
0
0.5
1
rho
B.
nCV
1.5
1
0.5
Normal
PDAC
Condition
Gene
BMAL1
CIART
CLOCK
CRY1
CRY2
DBP
NPAS2
NR1D1
PER1
PER2
PER3

A.

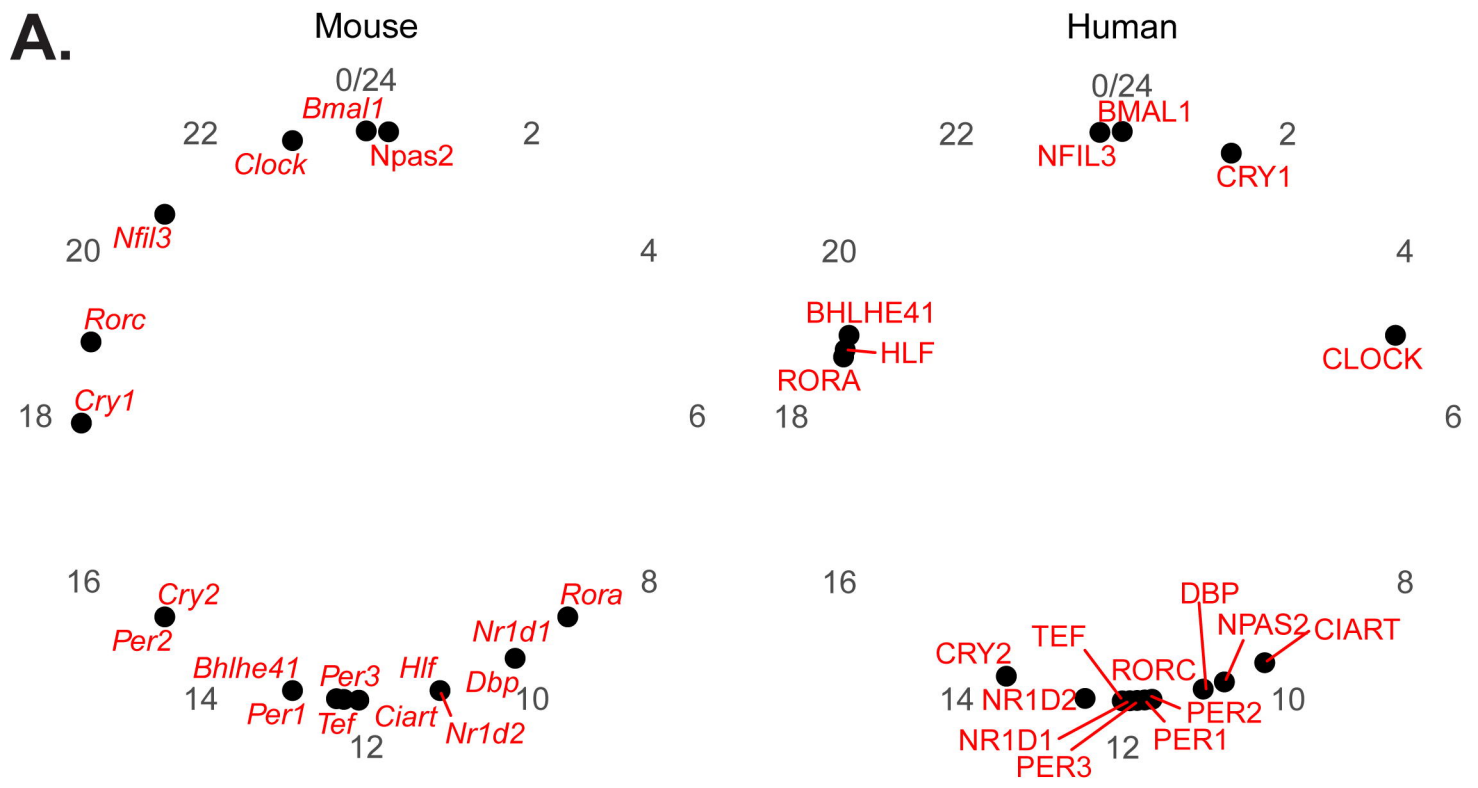

B.

Mouse Gene	Phase	Human Gene	Phase
Bmal1	0	BMAL1	0
Clock	23	CLOCK	4.9
Cry1	17.9	CRY1	1.5
Cry2	15	CRY2	13.6
Per1	13	PER1	11.7
Per2	15	PER2	11.6
Per3	12.4	PER3	11.8
Nr1d1	9	NR1D1	11.9
Nr1d2	11	NR1D2	12.5
Rora	9	RORA	18.8
Rorc	19	RORC	11.7
Npas2	0.3	NPAS2	10.6
Nfil3	21	NFIL3	23.7
Bhlhe41	13	BHLHE41	19.1
Dbp	9.9	DBP	10.9
Ciart	12.1	CIART	10
Tef	12.3	TEF	12
Hlf	11	HLF	18.9

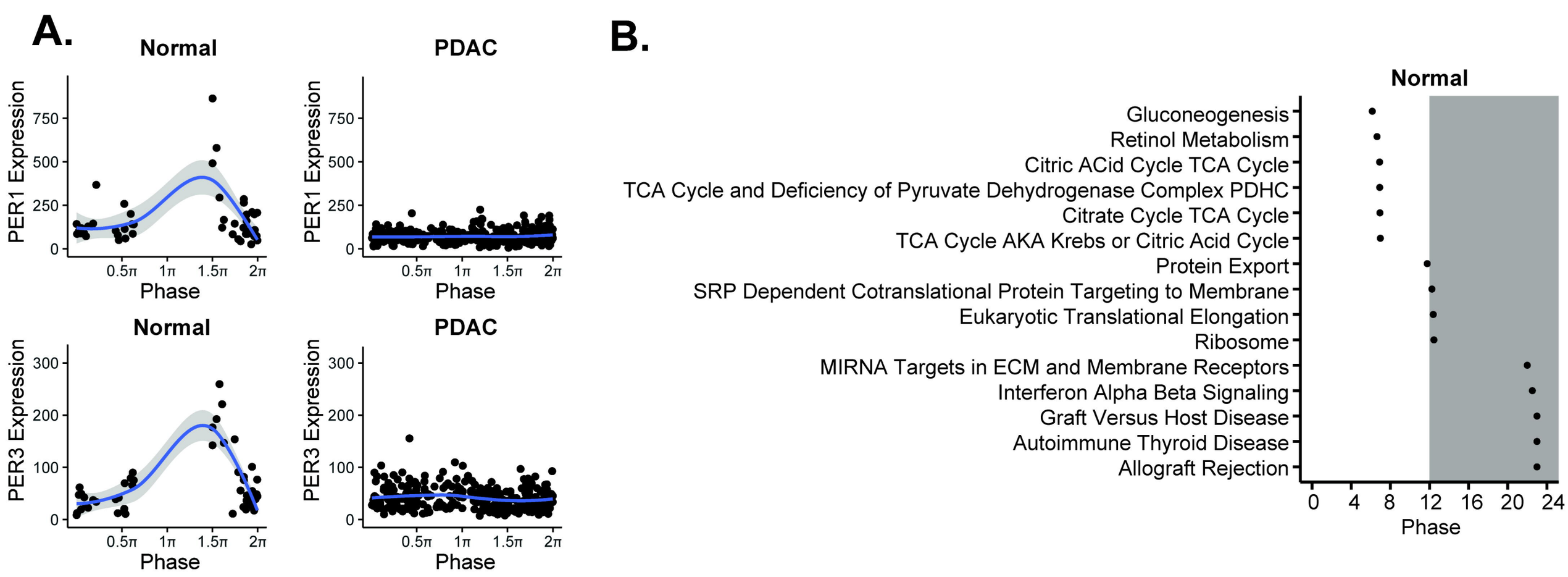
A.
Normal
PDAC
PER1 Expression
750
500
250
0
0.5π
1π
1.5π
2π
Phase
PER3 Expression
300
200
100
0
B.
Normal
Gluconeogenesis
Retinol Metabolism
Citric ACid Cycle TCA Cycle
TCA Cycle and Deficiency of Pyruvate Dehydrogenase Complex PDHC
Citrate Cycle TCA Cycle
TCA Cycle AKA Krebs or Citric Acid Cycle
Protein Export
SRP Dependent Cotranslational Protein Targeting to Membrane
Eukaryotic Translational Elongation
Ribosome
MIRNA Targets in ECM and Membrane Receptors
Interferon Alpha Beta Signaling
Graft Versus Host Disease
Autoimmune Thyroid Disease
Allograft Rejection
0
4
8
12
16
20
24
Phase

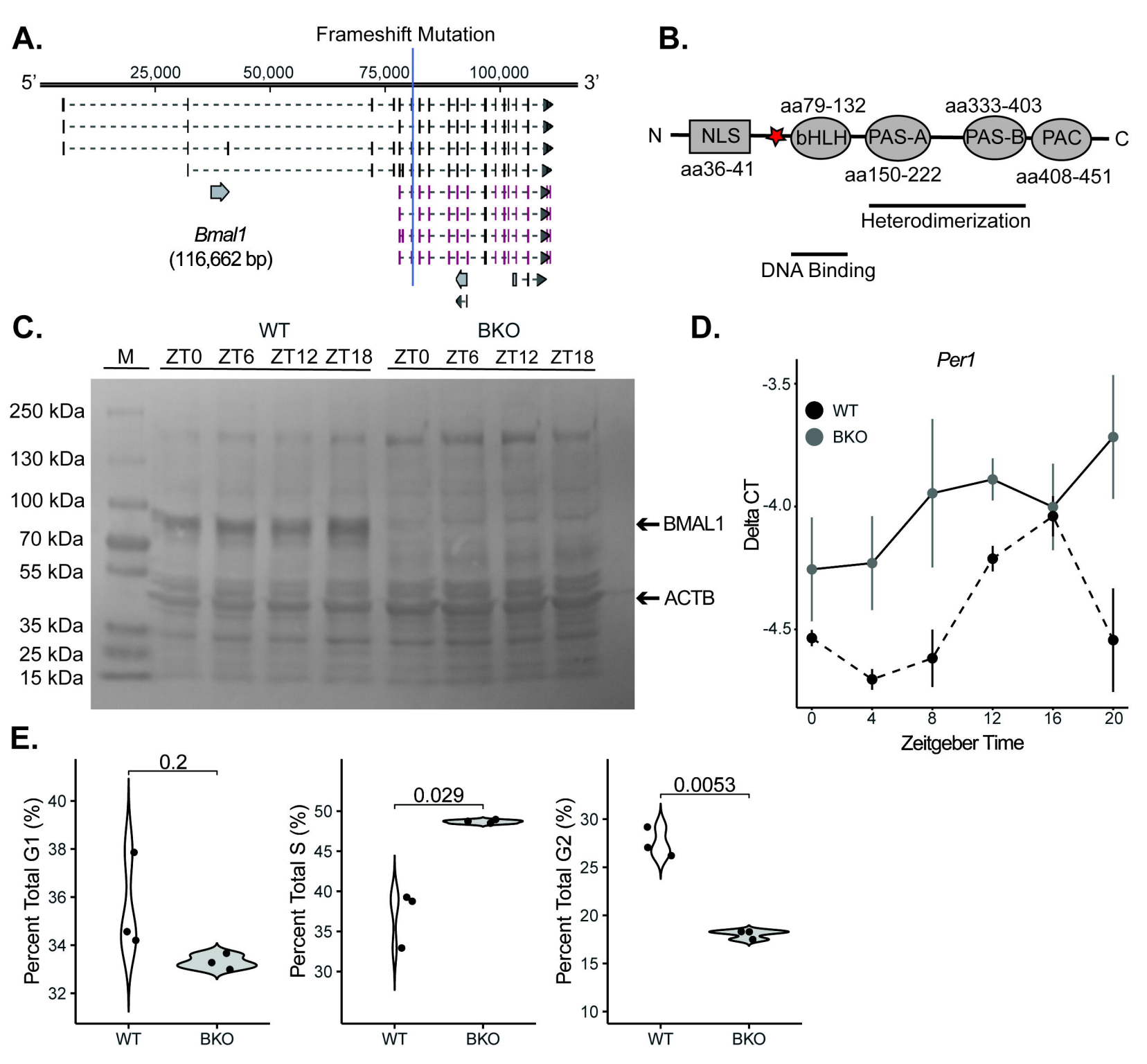
A.
Frameshift Mutation
5'
25,000
50,000
75,000
100,000
3'
Bmal1
(116,662 bp)
B.
N
NLS
aa36-41
aa79-132
bHLH
PAS-A
aa150-222
aa333-403
PAS-B
PAC
aa408-451
C
Heterodimerization
DNA Binding
C.
WT
BKO
M
ZT0 ZT6 ZT12 ZT18
ZT0 ZT6 ZT12 ZT18
250 kDa
130 kDa
100 kDa
70 kDa
55 kDa
35 kDa
25 kDa
15 kDa
BMAL1
ACTB
D.
Per1
WT
BKO
Delta CT
-3.5
-4.0
-4.5
0
4
8
12
16
20
Zeitgeber Time
E.
0.2
Percent Total G1 (%)
40
38
36
34
32
WT
BKO
0.029
Percent Total S (%)
50
45
40
35
30
WT
BKO
0.0053
Percent Total G2 (%)
30
25
20
15
10
WT
BKO

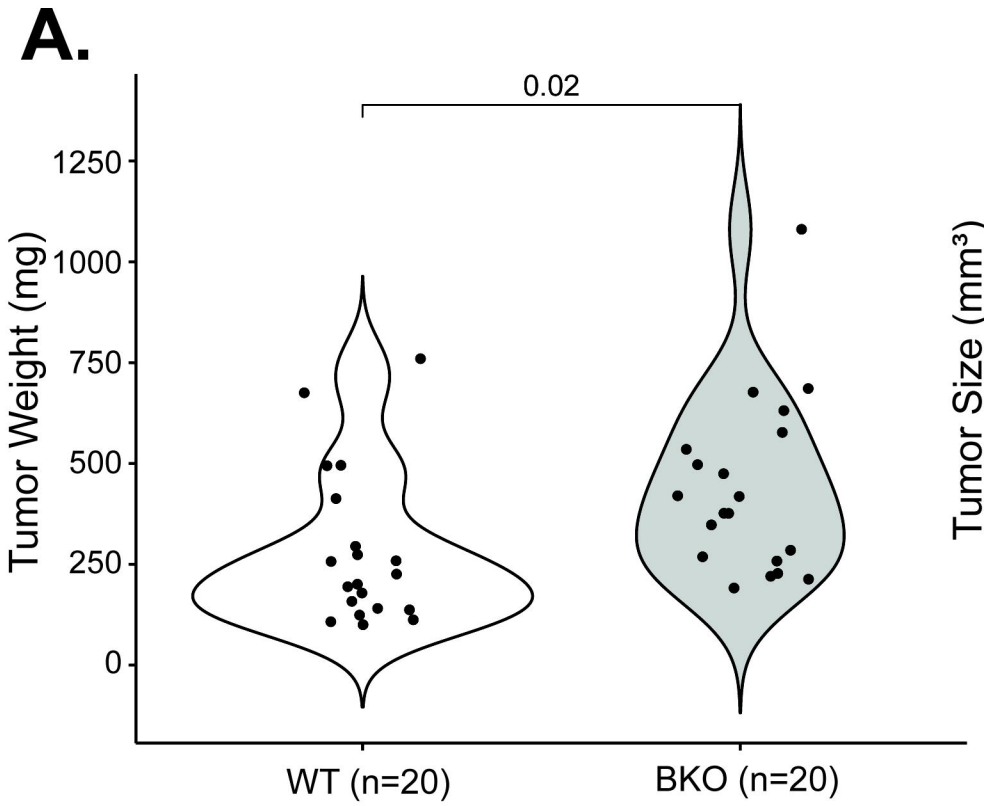
A.
0.02
Tumor Weight (mg)
1250
1000
750
500
250
0
WT (n=20)
BKO (n=20)

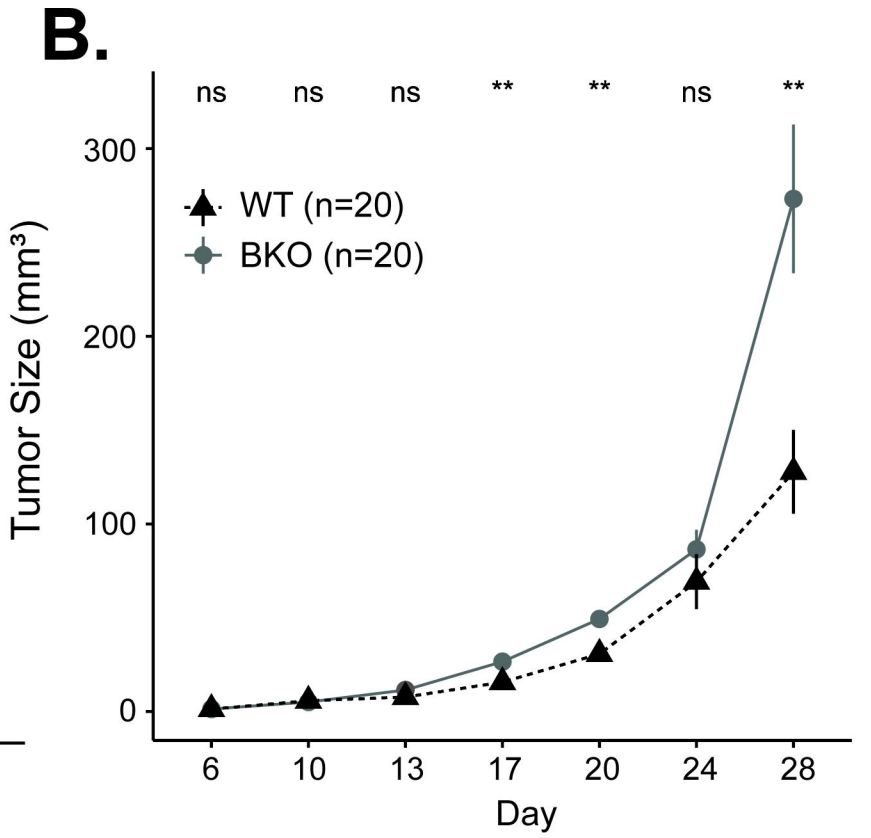
B.
ns
ns
ns
**
**
ns
**
Tumor Size (mm³)
300
200
100
0
WT (n=20)
BKO (n=20)
6
10
13
17
20
24
28
Day

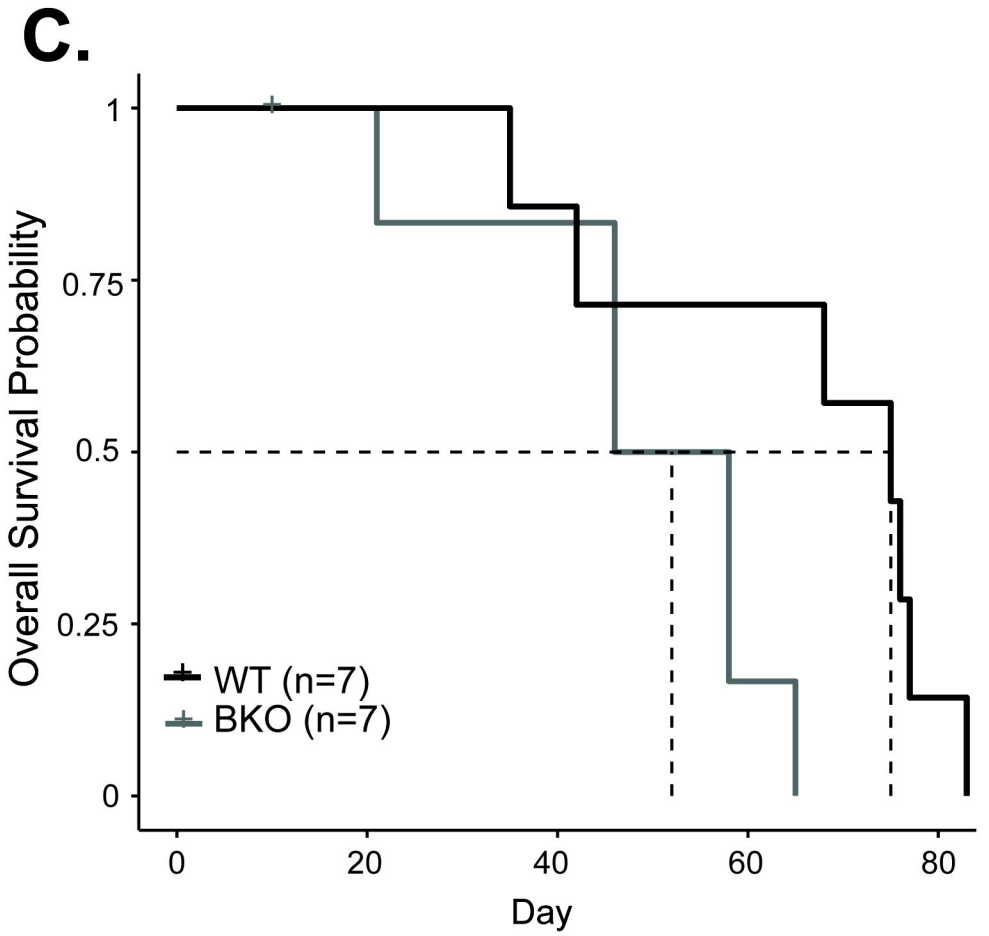
C.
Overall Survival Probability
1
0.75
0.5
0.25
0
WT (n=7)
BKO (n=7)
0
20
40
60
80
Day

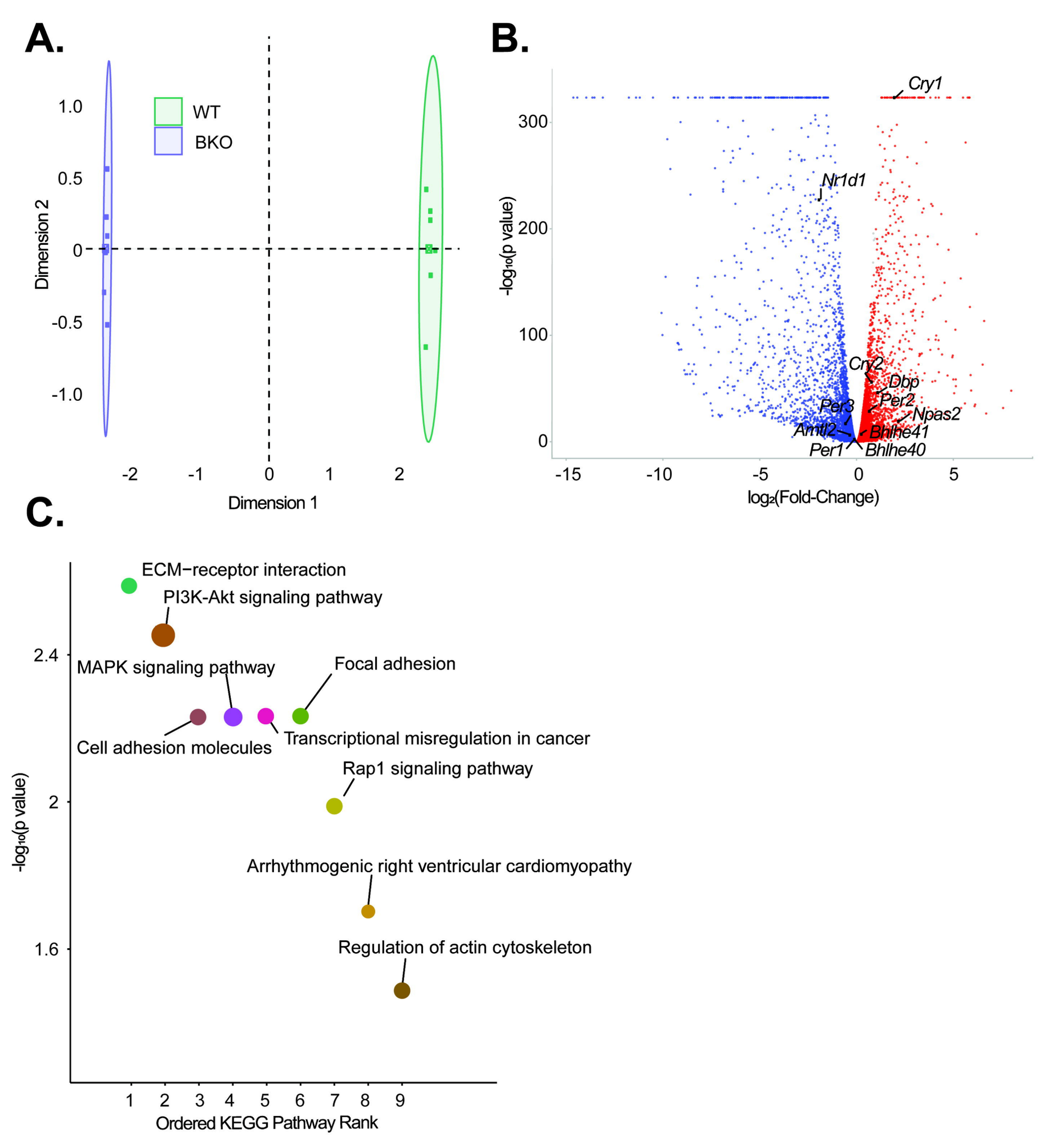
A.
WT
BKO
Dimension 2
Dimension 1
1.0
0.5
0
-0.5
-1.0
-2
-1
0
1
2
B.
Cry1
Nr1d1
Cry2
Dbp
Per2
Per3
Npas2
Amtl2
Bhlhe41
Per1
Bhlhe40
-log10(p value)
log2(Fold-Change)
300
200
100
0
-15
-10
-5
0
5
C.
ECM−receptor interaction
PI3K-Akt signaling pathway
MAPK signaling pathway
Focal adhesion
Cell adhesion molecules
Transcriptional misregulation in cancer
Rap1 signaling pathway
Arrhythmogenic right ventricular cardiomyopathy
Regulation of actin cytoskeleton
-log10(p value)
2.4
2
1.6
1
2
3
4
5
6
7
8
9
Ordered KEGG Pathway Rank

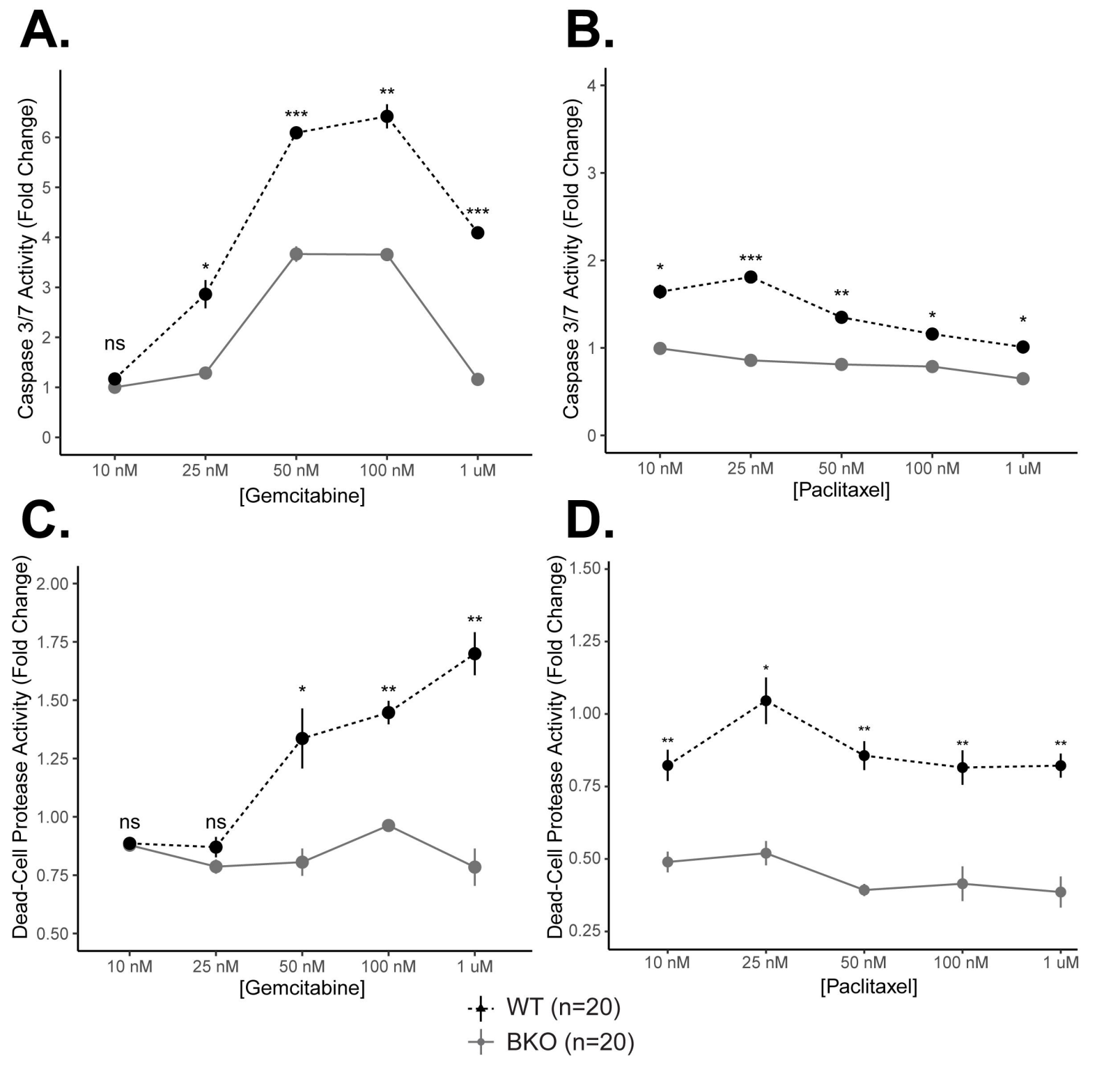
A.
Caspase 3/7 Activity (Fold Change)
0
1
2
3
4
5
6
ns
*
***
**
***
10 nM
25 nM
50 nM
100 nM
1 uM
[Gemcitabine]
B.
Caspase 3/7 Activity (Fold Change)
0
1
2
3
4
*
***
**
*
*
10 nM
25 nM
50 nM
100 nM
1 uM
[Paclitaxel]
C.
Dead-Cell Protease Activity (Fold Change)
0.50
0.75
1.00
1.25
1.50
1.75
2.00
ns
ns
*
**
**
10 nM
25 nM
50 nM
100 nM
1 uM
[Gemcitabine]
D.
Dead-Cell Protease Activity (Fold Change)
0.25
0.50
0.75
1.00
1.25
1.50
**
*
**
**
**
10 nM
25 nM
50 nM
100 nM
1 uM
[Paclitaxel]
WT (n=20)
BKO (n=20)